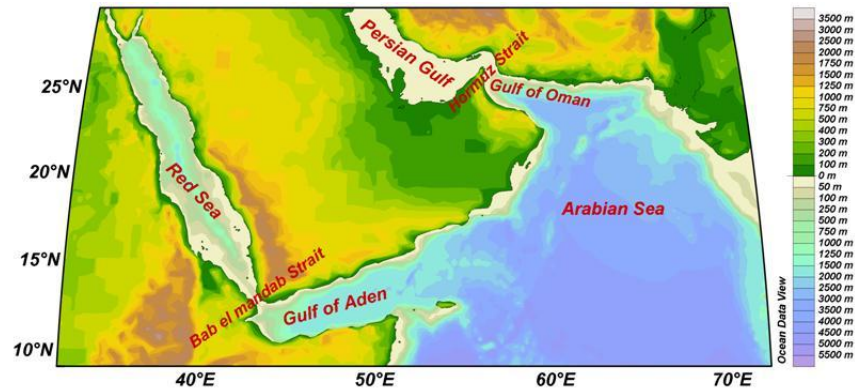


Factors controlling the total alkalinity in the Arabian Sea and Red Sea



by

Salma Kh. Elageed

A thesis submitted in partial fulfillment for the
degree of Master of Science in the



Faculty of Mathematics and Natural Sciences
Geophysical Institute
Chemical Oceanography

June 2010

©Elageed

UNIVERSITY OF BERGEN
Faculty of Mathematics and Natural Sciences
Geophysical Institute

Master of Science

by

Salma Kh. Elageed

Abstract

Based on data obtained during the Geochemical Ocean Section Study (*GEOSECS*) 1977, Mer Rouge (*MEROU*) 1982, and US Joint Global Ocean Flux (*JGOFs*) 1995 studies we have analyzed the processes controlling the total alkalinity (*TA*) of the whole water column in the Arabian Sea and the Red Sea. The main processes important for the *TA* variability in area of study are salinity variations, soft tissue production, calcium carbonate formation and dissolution, and sedimentation. For the subsurface waters different processes dominate in the different basins.

Regarding spatial variations in surface *TA*, maximum values occur in the Red Sea and minimum in the upwelling region along the Omani coast in the Arabian Sea. These variations are mainly associated with physical processes that control salinity.

Alkalinity variations were decomposed to contributions arising from salinity variations (ΔTA^s), organic matter production/remineralisation (ΔTA^{org}), and production/dissolution of calcium carbonate (ΔTA^{CaCO_3}). Positive Δ values resulted for the processes that increase *TA* whereas negative Δ values resulted for the processes that decrease *TA*. In the upper 200 m of the water column, (ΔTA^s) was found to be $70 \mu\text{mol kg}^{-1}$ and $121 \mu\text{mol kg}^{-1}$ for the Arabian Sea and the Red Sea, respectively. Below the 200 m depth the ΔTA^s was $45 \mu\text{mol kg}^{-1}$ and $6 \mu\text{mol kg}^{-1}$ for the Arabian Sea and the Red Sea respectively. ΔTA^{org} was maximum in surface ($24 \mu\text{mol kg}^{-1}$) for both Seas. For depths below 200 m, ΔTA^{org} was between -10 and $0 \mu\text{mol kg}^{-1}$ in the Arabian Sea, and between 0 and $10 \mu\text{mol kg}^{-1}$ in the Red Sea. Values for ΔTA^{CaCO_3} were around $0 \mu\text{mol kg}^{-1}$ in the surface in both

regions, but $\Delta\text{TA}^{\text{CaCO}_3}$ increased nearly linearly with depth in the Arabian Sea until it reached and stabilized to values around $150 \mu\text{mol kg}^{-1}$ at about 3000 m. The increase was due to dissolution of calcium carbonate (CaCO_3) as the Arabian Sea was found to be undersaturated with respect to aragonite and calcite around 400 and 3000 m, respectively. Conversely, the level of undersaturation was never reached in the Red Sea. Thus, sedimentation of CaCO_3 out of the water column was possible in the Red Sea. The fact that $\Delta\text{TA}^{\text{CaCO}_3}$ decreased and stabilized to a value of $-40 \mu\text{mol kg}^{-1}$ at about 500 m depth in the Red Sea suggested that CaCO_3 formation and sedimentation removed TA from the water column.

Acknowledgements

I first of all express my sincerest thanks to Almighty Allah for granting me the strength for completing this research. Certainly there is no might and no power except with Almighty Allah.

The careful guidance, valuable suggestions and tireless efforts of Truls Johannessen, Abdirahman M. Omar, and Ingunn Skjelvan during my research have been outstanding. This is the opportunity for me to express my heartfelt thanks to Eva Falck and Knut Barthel for their timely and fatherly guidance. Great thanks to Dr. Abdelgadir Dafalla Elhag and Institute of Marine Research staff and Faculty of Marine Sciences in Port Sudan for encouraging me to do this master study. Lastly and no sense the least I am thankful to Bjerknes Centre for Climate Research, Geophysical institute, and University of Bergen for extending all facilities and providing financial support to carry out this research.

Acknowledgement is to my family for their patience and support over the years, providing encouragement and support throughout my MSc research and for that I am very grateful. I am thankful for friends and colleagues in Bergen who helped me in different phases, keeping me out of the homesick feeling during my stay at the University of Bergen, without them I couldn't continue.

Contents

Abstract	i
Acknowledgements	iii
Contents	iv
List of Figures	vi
List of Tables	x
1 Aim of study	1
2 Description of location and hydrography	3
2.1 Arabian Sea	7
2.1.1 Hydrographic condition	8
2.1.2 Chemical condition	12
2.2 Red Sea	14
2.2.1 Hydrographic condition	16
2.2.2 Chemical and biological conditions	21
3 Ocean carbon cycle	24
4 Processes controlling alkalinity	30
4.1 Alkalinity changes due to physical processes	31
4.2 Alkalinity changes due to biogeochemical processes	32
4.2.1 Assimilation and remineralization of nutrients	32
4.2.2 Calcium carbonate formation, precipitation, and dissolution	34
5 Data sets and methodology	39
5.1 Data sets	39
5.1.1 JGOFS Cruises data 1995	40

5.1.2	GEOSECS data 1977	41
5.1.3	MEROU cruise data 1982	41
5.2	Methods	44
6	Result and discussion	47
6.1	Salinity control on TA	47
6.2	Impact of organic matter on TA	50
6.3	CaCO ₃ cycle and saturation depths	54
7	Summary of results	58
	Bibliography	60

List of Figures

2.1	Map of the area of study including bathymetry.	3
2.2	Surface winds during (a) summer and (b) winter, seasons in the Arabian Sea and southern Red Sea (from Lee et al., 2000).	4
2.3	Circulation in the Arabian Sea in (a) winter and (b) summer. Abbreviations are NEC, North Equatorial Current; SC, Somali Current; WICC, West India Coastal Current; EAC, East Arabian Current; IMC, Indian Monsoon Current; GW, Great Whirl; SE, Socotra Eddy; LH, Lakshadwee High; and LL, Lakshadweep Low. LH (LL) forms in the vicinity of the Lakshadweep Islands chain during winter (summer) (from Prasad et al., 2001).	5
2.4	Major barometric pressure systems and prevailing wind patterns over the Red Sea and the Intertropical Convergence Zone (ITCZ) during (a) summer and (b) winter (from Bonfil and Abdallah, 2004).	6
2.5	Map of the Arabian Sea and its bathymetry.	7
2.6	Levitus climatology of (a) summer mixed layer depth (MLD) and (b) winter MLD. (c) and (d) are schematic representations of the various physical processes that may act during summer and winter, respectively (from Lee et al., 2000).	9
2.7	SST in the Arabian Sea during (a) summer, and (b) winter, from an AVHRR (Advanced Very High Resolution Radiometer) image (http://www.rsmas.miami.edu/personal/eryan/arabian-sst/catalog.html). (c) shows summer temperatures in the Arabian Sea water column (from Tomczak and Godfrey, 2001).	10
2.8	T-S diagram of Arabian Sea water masses. The black lines, dashed lines, and grey lines correspond to the Gulf of Aden, Arabian Sea, and Bay of Bengal sections, respectively. The water-sources are indicated by white circles. BBSW, Bengal Bay Surface Water; ASW, Arabian Sea surfaceWater; RSSW, Red Sea SurfaceWater; IIW, Indian Intermediate Water; BBIW, Bengal Bay Intermediate Water; RSW, Red Sea Water; DIW, Deep Indian Water; BW, BottomWater (from Goyet et al., 1999).	11

2.9	Typical O ₂ profiles in the Arabian Sea, data from JGOFS 1995 (see chapter 5).	12
2.10	Seasonal variability of nutrients in the upper 50 m in the Arabian Sea. Winter distribution (a) and (c), summer distribution (b) and (d) of nitrate and phosphate, respectively. Data from JGFOS cruises, 1995 (see Chapter 5).	13
2.11	NO ₃ profiles in the Arabian Sea, data from JGOFS 1995 (see chapter 5).	14
2.12	Map of the Red Sea and the Gulf of Aden. Also shown are the states bordering the Red Sea.	15
2.13	General bathymetry of the Red Sea and Gulf of Aden.	16
2.14	The mean surface circulation in the Red Sea during (a) winter and (b) summer, from MICOM simulation (Sofianos and Johns, 2003).	17
2.15	Schematic of the (a) winter and (b) summer water exchange regimes in the strait of Bab el Mandeb, where GASW is Gulf of Aden Surface Water, RSW is Red Sea Surface Water, GAIW is Gulf of Aden Intermediate Water, RSDW is Red Sea Deep Water, and RSOW is Red Sea Overflow Water (from Siddall et al., 2002).	18
2.16	Distribution of potential temperature (°C) in the Red Sea (a) surface and (b) water column (from Sofianos and Johns, 2003).	19
2.17	Salinity distribution in the Red Sea (a) surface water and (b) water column (from Sofianos and Johns, 2003; Tomczak and Godfrey, 2001).	20
2.18	Sketch of the Red Sea circulation (Jean-Baptiste et al., 2004).	20
2.19	Hydrographic section of oxygen (ml l ⁻¹) in the Red Sea during winter (1 ml l ⁻¹ is equivalent to about 43.6 μmol kg ⁻¹ , assuming a density of 1.025 kg l ⁻¹).	22
2.20	Map of the Red Sea coral reef distribution (from Kotb et al., 2004).	23
3.1	Global carbon cycle. Numbers in black are preindustrial and red are those influenced by human activities. Numbers inside the earth compartments are the respective reservoir sizes and those next to arrows are rates of carbon transfer. Black arrows indicate estimated rates for preindustrial era whereas red arrows account for anthropogenically modified rates. Red numbers within brackets are the accumulation rates of anthropogenic carbon dioxide in atmosphere and oceans in Gt y ⁻¹ (Gt C = 10 ¹⁵ g C) (from http://www.whrc.org/carbon/index.htm).	24
3.2	Concentrations of the different inorganic carbon species as a function of pH. Equilibrium constants for equations 3.2 and 3.3 are indicated in the figure (from Sarmiento and Gruber, 2006).	27
3.3	A sketch showing different pumps transporting CO ₂ between atmosphere and ocean, and also within the ocean (from Heinze et al., 1991).	28

3.4	Global map of the average annual exchange of CO_2 ($\text{mol C m}^{-2} \text{y}^{-1}$) across the sea surface (from http://oceanworld.tamu.edu/resources/oceanography-book/carboncycle.htm).	28
4.1	A sketch showing how different processes affect DIC and TA. TA varies mainly with formation and dissolution of calcium carbonate (from Zeebe and Wolf-Gladrow, 2001).	30
4.2	Monthly mean values of surface TA ($\mu\text{mol kg}^{-1}$) for (a) January and (b) July for the world's ocean, as estimated from http://cdiac.ornl.gov/oceans/SurfaceAlkalinityClimatology_ODV/Climatology_ODV.html .	32
4.3	The main calcifying groups in the ocean and their generation time.	34
4.4	The crystalline structure of (a) aragonite (Ar) and (b) calcite (Ca).	35
4.5	Carbonate concentrations versus depth and carbonate saturation with respect to aragonite (dashed line) and calcite (solid line) for the south Atlantic (a) and north Pacific (b) (from Sarmiento and Gruber, 2006).	37
4.6	A global picture of the saturation depth ($\Omega=1$) for (a) aragonite and (b) calcite (from Feely et al., 2004).	38
5.1	A map of the Arabian Sea and the Red Sea with stations indicated.	39
5.2	Stations collected at the JGOFS Arabian Sea cruises during (a) winter and (b) summer.	40
5.3	GEOSECS 1977 stations in the Red Sea and Gulf of Aden.	41
5.4	MEROU 1982 cruises in the Red Sea.	42
6.1	Surface TA and SSS during summer (a) and (b) and winter (c) and (d) in the Red and the Arabian Sea.	48
6.2	(a) Relationship between TA and salinity in the upper 50 m and (b) vertical distribution of salinity.	49
6.3	Relationship between TA and NO_3 in the depth range 50–600 m in the (a) Arabian Sea and (b) Red Sea.	51
6.4	Change in alkalinity due to production/remineralisation of organic matter, ΔTA^{org} in the Arabian Sea and Red Sea.	51
6.5	Surface DIC and nitrate during (a and b) summer and (c and d) winter in the Red and Arabian Seas.	52
6.6	C: N and C: P ratios in the Arabian Sea (a and c) and the Red Sea (b and d). The colour indicates Oxygen concentration.	53
6.7	Degree of saturation with respect to aragonite during (a) summer and (b) winter in the Red Sea and the Arabian Sea.	55
6.8	Degree of saturation with respect to calcite during (a) summer and (b) winter in the Red Sea and the Arabian Sea.	55

6.9	Depth profiles of the degree of saturation (Ω) of (a) aragonite and (b) calcite in the Arabian Sea and Red Sea. The Red lines indicate that the degree of saturation equals One.	56
6.10	(a) nTA and (b) ΔTA^{CaCO_3} as function of depth in the Red Sea and the Arabian Sea. The colour indicates longitude.	56
6.11	(a) $nDIC$ as a function of depth and (b) relation between carbon loss and temperature in upper 160 m in the Red Sea and Arabian Sea. The colour indicates longitude.	57

List of Tables

2.1	Basic information about Arabian Sea	8
2.2	Basic information of the Red Sea region, modified from Ali (2008). . .	16
5.1	Summary of the Arabian and Red Seas datasets	43
6.1	Mean values and standard deviations for the salinity (S), total alkalinity (TA), nitrate (NO_3), and total carbon (DIC) for the source water. Also shown are slopes (a) and intercepts (b) for TA^{cor} verses S relationships in the Arabian Sea and the Red Sea.	50

to
my parents
and to
Mohammed and Sara
with my love

Chapter 1

Aim of study

Alkalinity is one of the most geochemically interesting parameters characterizing the carbon chemistry. It is defined in different ways for different applications, but in general it is a measure of how much acid (H^+) is required to lower the pH to a specific level. One particular reason to study alkalinity is that when organisms build calcium carbonate skeletons, they take up calcium and carbonate from the water column. Coral reefs and other calcifying marine ecosystems, such as calcareous marine algae are directly threatened by the global increase of atmospheric carbon dioxide ([Kempe and Kazmierczak, 1994](#); [Langdon et al., 2000](#)). This is because the absorption of fossil fuel CO_2 in the ocean also consumes carbonate ions from the water column. Thus, CO_2 emissions can modify the chemistry of oceanic surface waters by decreasing the calcium carbonate saturation, and this can hamper the growth of corals and other calcareous organisms. Such changes in the ocean calcification would result in total alkalinity (TA) changes, and in order to detect them we need to know about –and account for– TA variations resulting from other processes. Beside being intimately connected with the chemistry of formation/dissolution of calcium carbonate ($CaCO_3$), TA is also a sensitive indicator for physical processes such as ocean mixing, evaporation and weathering, in addition to being slightly influenced by organic matter production and oxidation.

The presence of landmass to the Arabian Sea makes it vibrant with the occurrence of tropical monsoons. It is a very biologically productive region due to mixing processes driven by summer and winter monsoons which induce higher production

in the Arabian Sea than in the Red Sea. Higher biological productivity in surface waters leads to oxygen deficiency in middle layers of the water column in the Arabian Sea. Bacterial decomposition of organic matter under oxygen deficient conditions is carried out through nitrate reduction and denitrification (Kumar, 2006; Morrison et al., 1999). Some of the low oxygen water is transported into the Red Sea, although active denitrification does not take place there. Arabian and Red Seas are sources for atmospheric carbon due to warm surface waters that are CO₂ supersaturated (Ali, 2008; Kumar, 2006).

A significant fraction of the carbon dioxide (CO₂) released to the atmosphere as a result of human activity is taken up by the ocean (Egleston et al., 2010). As a result of this uptake, the marine carbonate chemistry is currently changed and is expected to be perturbed even more in the future (e.g., Feely et al., 2004; Kleypas and Langdon, 2006; Wolf-Gladrow et al., 1999). This can produce changes in biological processes of the ocean, which by themselves can lead to further perturbations in the marine chemistry. For instance, changes in marine calcification due to ocean acidification can lead to changes in TA, which is an indicator for the capacity of seawater to dissolve and hold CO₂ (Goyet et al., 1999). The aim of this thesis is to study the spatiotemporal distribution of TA in the Red Sea and the Arabian Sea, which both lie in the tropics where the largest changes of TA due to anthropogenic calcification changes are expected to be detected in the future (Ilyina et al., 2009; Schulz et al., 2009; Zondervan et al., 2001).

Description of location and hydrography

The Red Sea and Arabian Sea (Figure 2.1) are situated in the tropical belt within an unique environment. The Red Sea is an inland semi-enclosed sea while Arabian Sea is bounded in the north by land masses. The Red Sea is in an arid zone with high evaporation, no permanent rivers flow into the sea, and rainfall is rare.

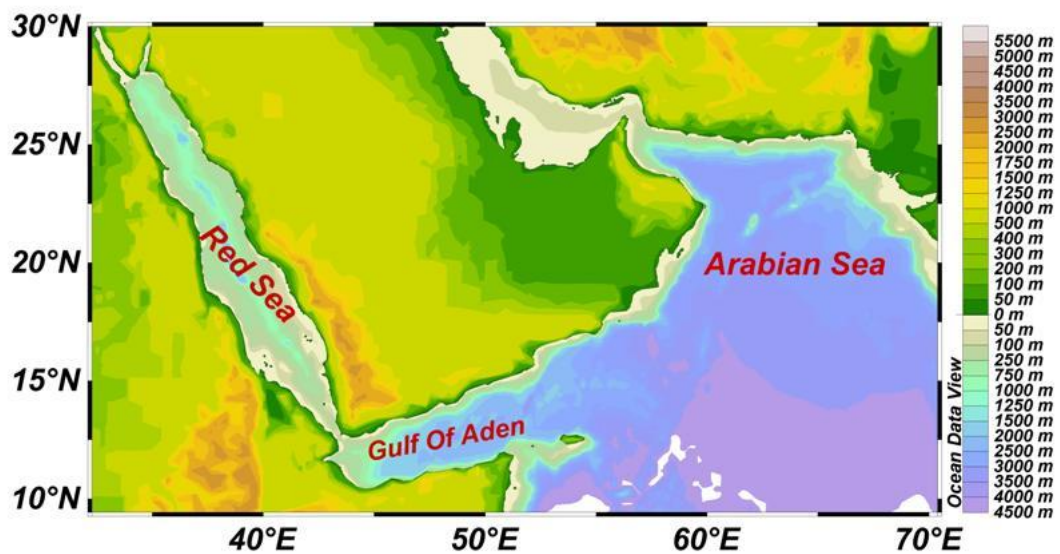


FIGURE 2.1: Map of the area of study including bathymetry.

Arabian Sea, Gulf of Aden, and the southern part of the Red Sea are affected by the same climatic monsoon system (Aiki et al., 2006), while the northern part of Red Sea is affected by Mediterranean climate. In summer, heating of the land produces a region of intense low surface pressure over northwestern India, Pakistan, and northern Arabia which produce strong winds ($\sim 15 \text{ m s}^{-1}$), coming from a southwesterly direction, called the southwest monsoon (SW) (Dickey et al., 1998). In winter (Figure 2.2), when the Eurasian continent cools, a high pressure region develops on the Tibetan plateau and northeast winds persist over the Arabian Sea (Kumar, 2006; Smith and Madhupratap, 2005). These winds are not as strong as during summer ($\sim 5 \text{ m s}^{-1}$) and have a northeasterly direction, called the northeast monsoon (NE) (Dickey et al., 1998; Luis and Kawamura, 2004),

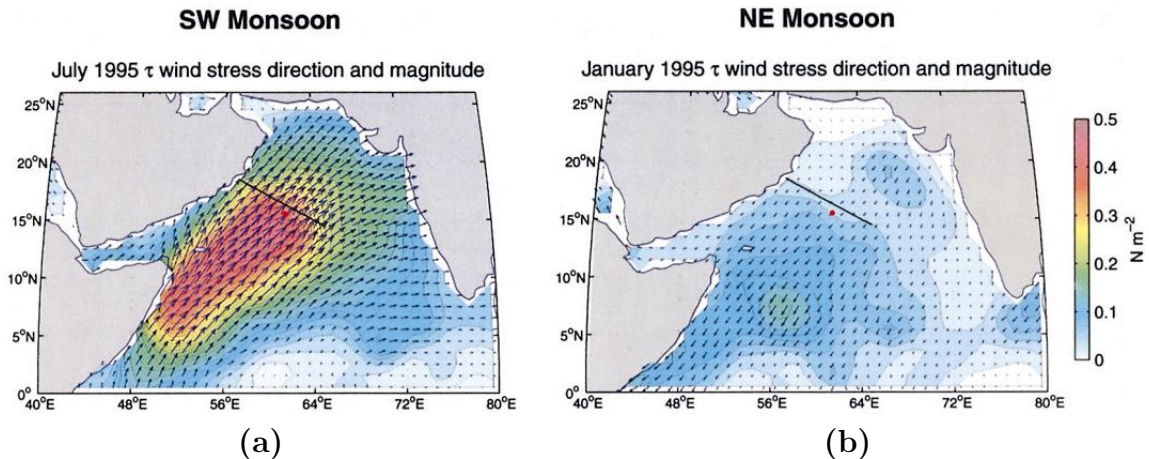


FIGURE 2.2: Surface winds during (a) summer and (b) winter, seasons in the Arabian Sea and southern Red Sea (from Lee et al., 2000).

The circulation changes in the upper layers of the Arabian Sea water column is a result of the semiannually and periodic reversals in the winds driving the Arabian Sea surface currents (Luis and Kawamura, 2004). During winter with northeasterly monsoon the North Equatorial Current (NEC) is flowing westward (Figure 2.3). The NEC bifurcates at the southeastern tip of India with a branch flowing northward as the West India Coastal Current (WICC). The northeasterly winds drive a southward boundary current along the coast of Somalia. South of the equator, these currents meet with the northward flowing East African Coastal Current (EACC) and flow offshore as a countercurrent. The flow in the interior Arabian Sea is westward. The NEC is replaced by the much stronger eastward flowing Indian Monsoon Current (IMC) during summer.

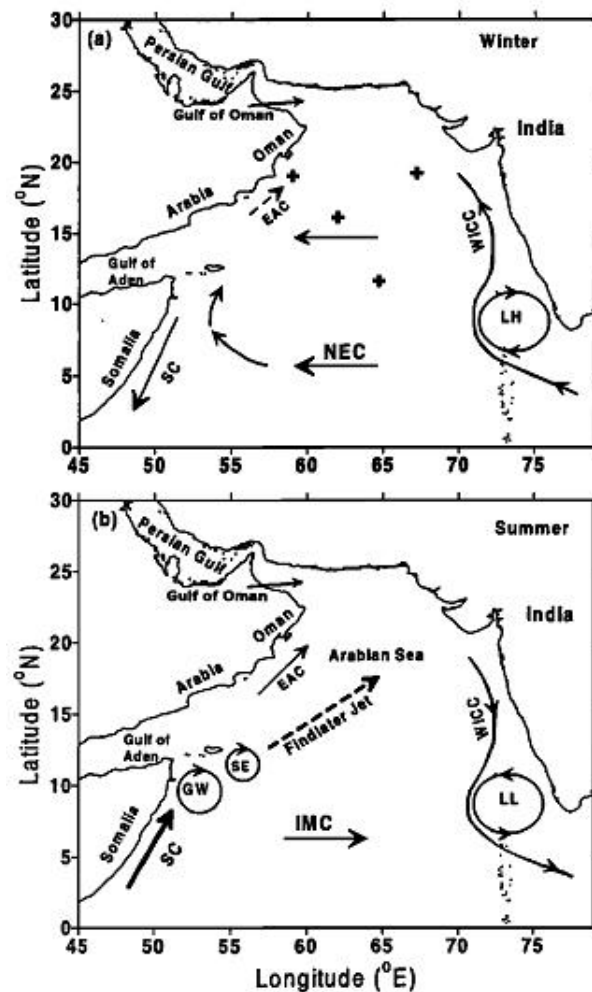


FIGURE 2.3: Circulation in the Arabian Sea in (a) winter and (b) summer. Abbreviations are NEC, North Equatorial Current; SC, Somali Current; WICC, West India Coastal Current; EAC, East Arabian Current; IMC, Indian Monsoon Current; GW, Great Whirl; SE, Socotra Eddy; LH, Lakshadweep High; and LL, Lakshadweep Low. LH (LL) forms in the vicinity of the Lakshadweep Islands chain during winter (summer) (from Prasad et al., 2001).

In the northern Red Sea (north of latitude 20°N) winds are predominantly from the north northwest, all year round. Only during winter months there are occasional southerly winds. The Red Sea south of 20°N is subject to the same annual monsoonal events as in the Arabian Sea (Bonfil and Abdallah, 2004). During the winter (October to May) the northeast monsoon blow into the Gulf of Aden and wind funnels up into the Red Sea from the southeast. During the summer (June to October) strong winds from the north northwest extend their influence over the southern Red Sea (Figure 2.4) which act against the southwest monsoon blowing

over the Gulf of Aden until they are deflected northeast up the southern coast of Arabia. These summer wind patterns drive a strong upwelling of deep, cold, nutrient-rich ocean water along the southern Arabian coastline. Coral growth is inhibited, but kelp beds thrive and productivity is high, reflected in the rich coastal fisheries (Bonfil and Abdallah, 2004).

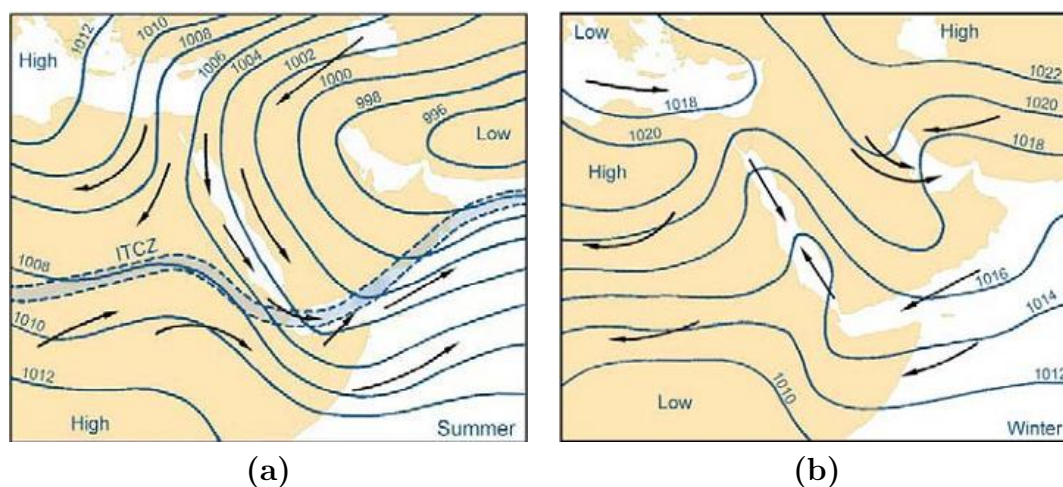


FIGURE 2.4: Major barometric pressure systems and prevailing wind patterns over the Red Sea and the Intertropical Convergence Zone (ITCZ) during (a) summer and (b) winter (from Bonfil and Abdallah, 2004).

Although the areas experience relatively similar climate, the hydrography is different. The ecosystems make the Red Sea internationally significant as the extensive and very beautiful coral reefs are inhabited by many species which occur nowhere else in the world. In contrast, there are no significant coral reefs in the Arabian Sea, but it is well known as an area of enhanced marine biological productivity as well as variability of the zooplankton due to an upwelling system driven by the southwesterly monsoon (Naqvi et al., 2005). In the south there is a permanent oxygen minimum zone between 200 and 1500 m due to a sluggish intermediate-depth circulation and microbial decay of the settling organic matter (Shimmield et al., 1990). In the following sections the seas will be presented separately.

2.1 Arabian Sea

The Arabian Sea, which in Roman times had the name Mare Erythraeum (Erythraean Sea), is located in the northwestern Indian Ocean. It is bounded by India to the east, Pakistan and Iran to the north, and the Arabian Peninsula in the west. It is connected with the Red Sea via the Gulf of Aden through Bab el Mandeb in the southwest and with the Persian Gulf through the Strait of Hormuz via the Gulf of Oman in the northwest. The Arabian Sea has a mean depth of 2,734 m. The Indus and the Narmada rivers are the principal waterways draining into the sea. The bathymetry of the Arabian Sea is shown in Figure 2.5 and basic information about the sea is presented in Table 2.1.

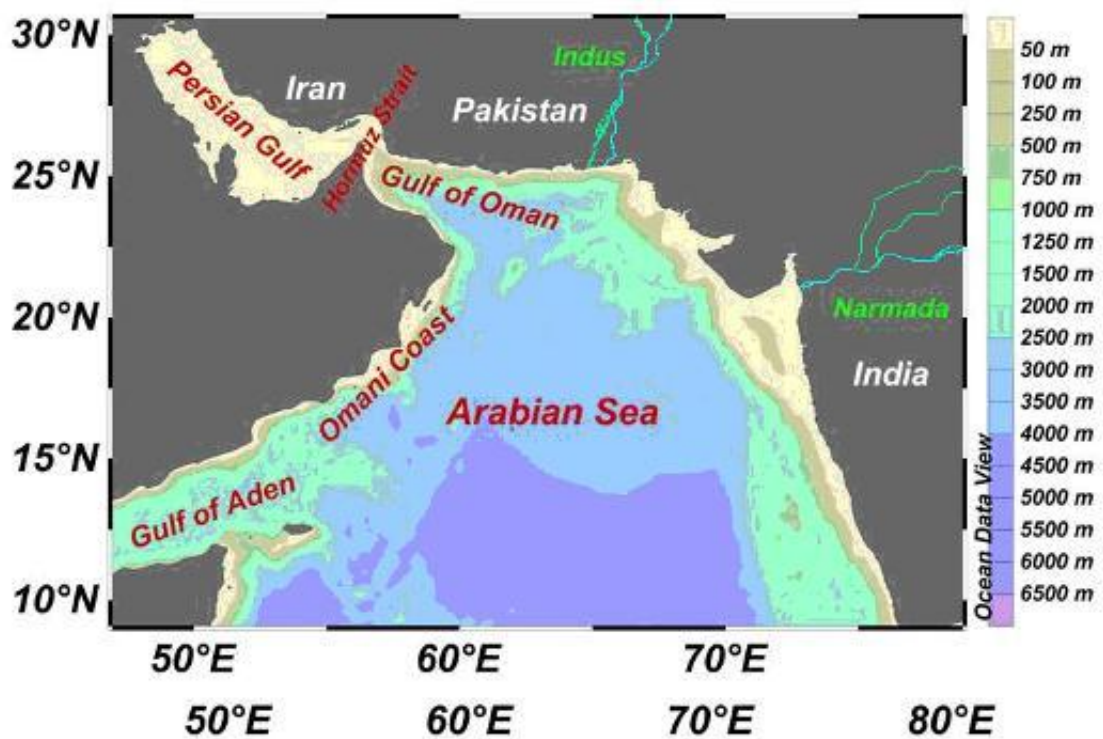


FIGURE 2.5: Map of the Arabian Sea and its bathymetry.

TABLE 2.1: Basic information about Arabian Sea

Parameter	Fact	Reference
Surface area	3862000 km ²	Abdel Aleem et al. (2009)
Volume	230560 km ³	Abdel Aleem et al. (2009)
Maximum width	2400 km	Abdel Aleem et al. (2009)
Maximum depth	4652 m	Abdel Aleem et al. (2009)
Length	110 km	Abdel Aleem et al. (2009)

2.1.1 Hydrographic condition

In general, the surface circulation in the Arabian Sea is anticyclonic during the SW monsoon with a broad eastward flow along the northern margin. Ekman transport towards the center of the northern Arabian Sea during the SW monsoon generally gives rise to a deepening of the mixed layer ([Brand and Griffiths, 2009](#)) which brings warm low salinity water into the Arabian Sea. Currents in the Arabian Sea basins evolve rapidly into a complex pattern of eddies as a result of strong horizontal temperature gradients and current shears. The winds drive the intense northeastward Somali Current along the coast of Somalia forming as a western boundary current whose speed can exceed 200 cm s⁻¹ ([Vecchi et al., 2004](#)). The Somali Current breaks into a chain of numerous quasi-stationary anticyclonic eddies that continue to the northeast. A general Ekman pumping takes place over a large portion of the Arabian Sea. The Ekman divergence in the northwest produces strong upwelling in the open ocean ([Garrison et al., 1998](#)) while Ekman convergence is dominant to the southeast of the Findlater Jet, causing shallow mixed-layers north of the Findlater Jet and much deeper mixed-layers to the south (Figures 2.6a and 2.6c).

In contrast to the southwest monsoon, the northeast monsoon (Figures 2.6b and 2.6d) form a broad flow without strong lateral gradients. Ekman pumping is found to be less important during this period, and mixing is identified as the dominant mechanism ([Lee et al., 2000](#)).

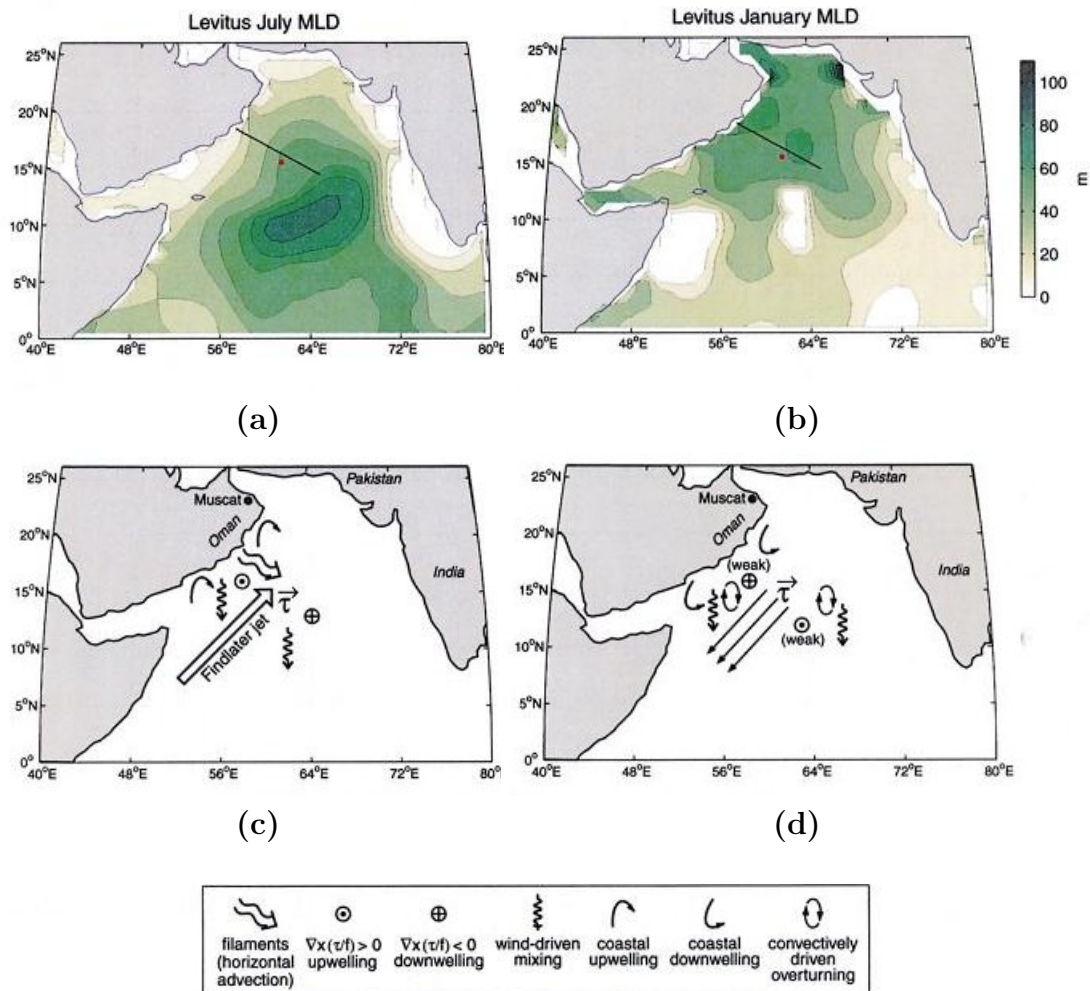


FIGURE 2.6: Levitus climatology of (a) summer mixed layer depth (MLD) and (b) winter MLD. (c) and (d) are schematic representations of the various physical processes that may act during summer and winter, respectively (from [Lee et al., 2000](#)).

Minimum sea surface temperatures (SST) of about 24 to 25°C ([Honjo and Weller, 1997](#)) occur in the central Arabian Sea during winter (NE monsoon) (Figure 2.7a), while SST increases southward exceeding 27.5°C to reach its maximum 28°C around 10°N as a result of southward flow in response to north-easterly winds ([Lee et al., 2000](#)) (Figure 2.7b). The strong upwelling at the Omani coast results in lower temperature here compared to open ocean (Figure 2.7c).

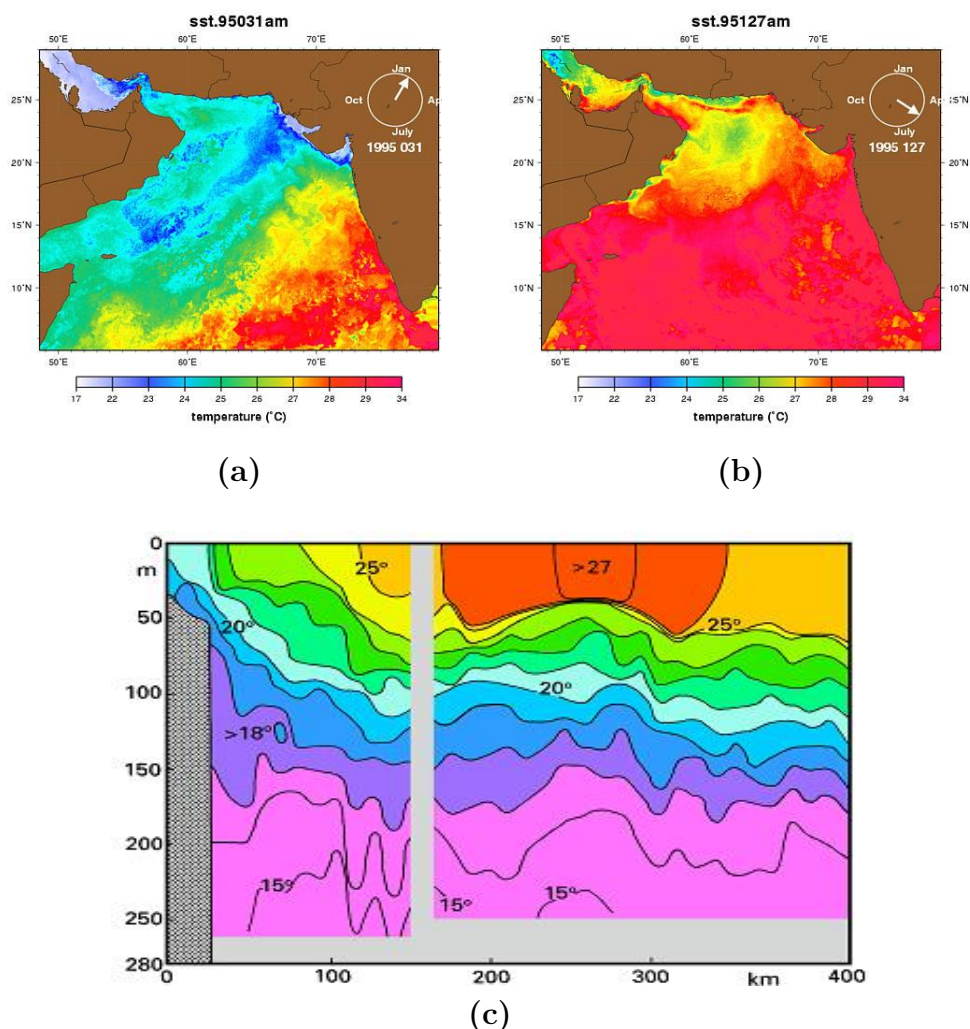


FIGURE 2.7: SST in the Arabian Sea during (a) summer, and (b) winter, from an AVHRR (Advanced Very High Resolution Radiometer) image (<http://www.rsmas.miami.edu/personal/eryan/arabian-sst/catalog.html>). (c) shows summer temperatures in the Arabian Sea water column (from Tomczak and Godfrey, 2001).

Generally speaking, the sea surface salinity (SSS) reflects the rainfall, runoff from land, and evaporation from the ocean surface. Annually the Arabian Sea exhibits a net water loss because evaporation exceeds the combined precipitation and riverine input to the region (Tomczak and Godfrey, 1994). The surface salinity is more than 36 all over the sea except during summer upwelling at the coast of Oman. During winter the highest SSS occurs in the northern region upper 50 m as the result of southward advection of highly saline surface waters from the Gulf of Oman and also strong evaporation associated with the northeast monsoon.

The upper waters of the northern Arabian Sea are dominated by two water masses (Brand and Griffiths, 2009; Luis and Kawamura, 2004), the Arabian Sea Water (ASW) and the Persian Gulf Water (PGW) (Figure 2.8). During the NE monsoon the continental winds will cool the high-salinity surface waters of the northern Arabian Sea, giving rise to the formation and sinking of the ASW. It sinks and spreads to form a salinity maximum just below the surface mixed layer and is identified with a core density $\sigma = 25 \text{ kg m}^{-3}$ (where σ is equal to the density minus 1000). The PGW enters the Arabian Sea from the Persian Gulf. It submerges below the ASW and spreads eastwards at a depth range of between 250 and 300 m, and it is characterized by a core density of 26.6 kg m^{-3} . The Red Sea Water (RSW) entering the Arabian Sea through the Gulf of Aden makes only a minor contribution to the water mass structure of the northern Arabian Sea. The RSW has a core density of 27.6 kg m^{-3} . The Indian Ocean Deep Water (IODW) forms the deepest water of the northern Arabian Sea. This oxygen-rich, relatively saline, and high-silicate water probably derives from the Circumpolar Deep Water of the Southern Ocean (Chowdary et al., 2005; Goyet et al., 1999; Prasad et al., 2001; Schott et al., 2001; Shetye et al., 1994).

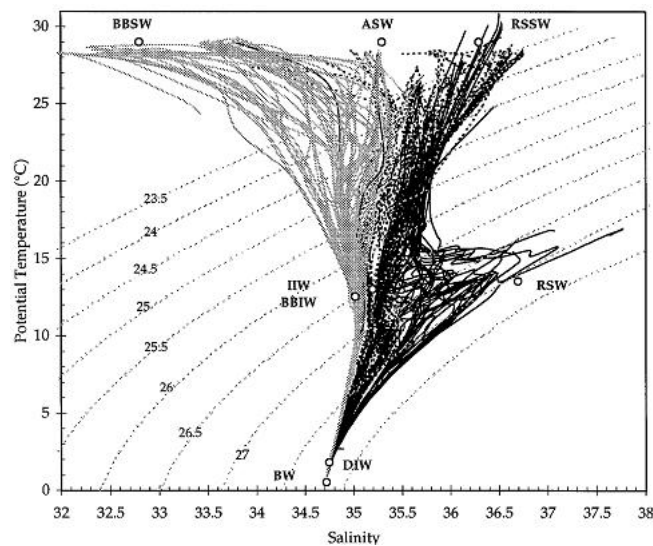


FIGURE 2.8: T-S diagram of Arabian Sea water masses. The black lines, dashed lines, and grey lines correspond to the Gulf of Aden, Arabian Sea, and Bay of Bengal sections, respectively. The water-sources are indicated by white circles. BBSW, Bengal Bay Surface Water; ASW, Arabian Sea surface Water; RSSW, Red Sea Surface Water; IIW, Indian Intermediate Water; BBIW, Bengal Bay Intermediate Water; RSW, Red Sea Water; DIW, Deep Indian Water; BW, Bottom Water (from Goyet et al., 1999).

2.1.2 Chemical condition

A characteristic feature of the Arabian Sea is the oxygen minimum zone (OMZ), which lies between 100 and 1000 m depth and which is most pronounced in the central and eastern Arabian Sea (Figure 2.9). The OMZ is maintained by limited deep water ventilation, high rates of water column respiration due to monsoon driven cycles of high productivity, and limited surface aeration due to a strong pycnocline between the ASW and PGW (Brand and Griffiths, 2009; Smith and Madhupratap, 2005). The lowest oxygen concentrations at these depths can be found in winter when minimum values reach near zero levels in the coastal areas while in the open ocean the values are about $15 \mu\text{mol l}^{-1}$ (De Pol-Holz et al., 2009; Morrison et al., 1999).

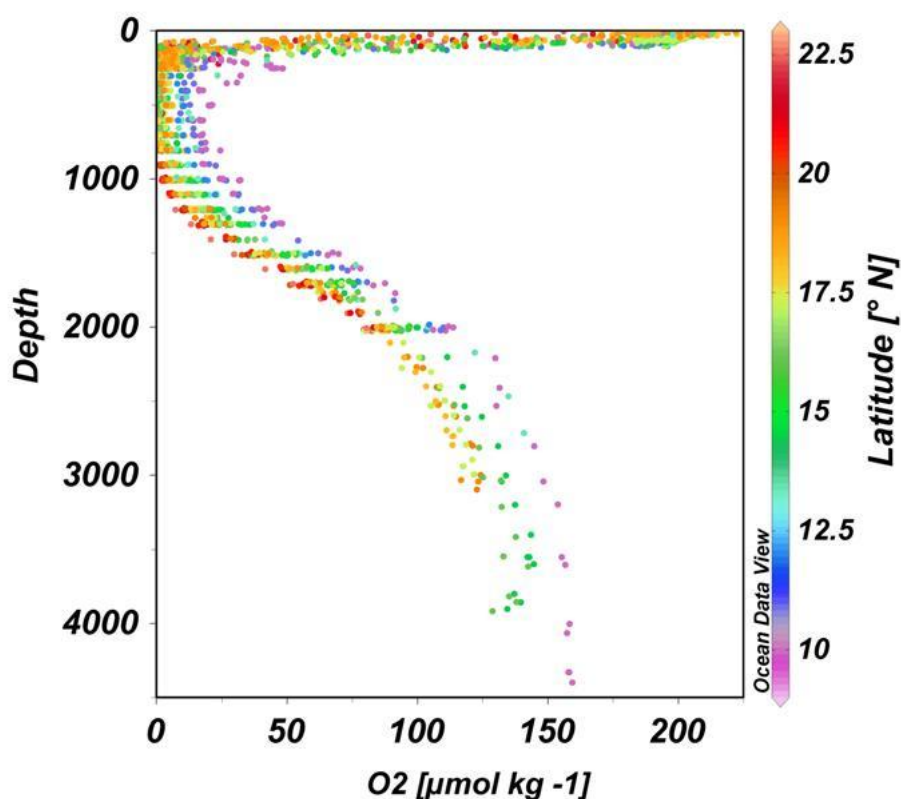


FIGURE 2.9: Typical O_2 profiles in the Arabian Sea, data from JGOFS 1995 (see chapter 5).

The distribution of nutrients concentrations in the Arabian Sea vary with season, latitude, and depth, shown in Figure 2.10. In summer there is a conspicuous high nutrients patch in surface waters along the Omani coast which is characterized

by lower temperature due to upwelling resulting from gyral circulation (DeSousa et al., 1996), whereas surface waters were devoid of nutrients in winter. The distributions of nitrate are about $2 \mu\text{mol l}^{-1}$ in the surface waters of northern latitudes resulting from winter cooling and convective mixing.

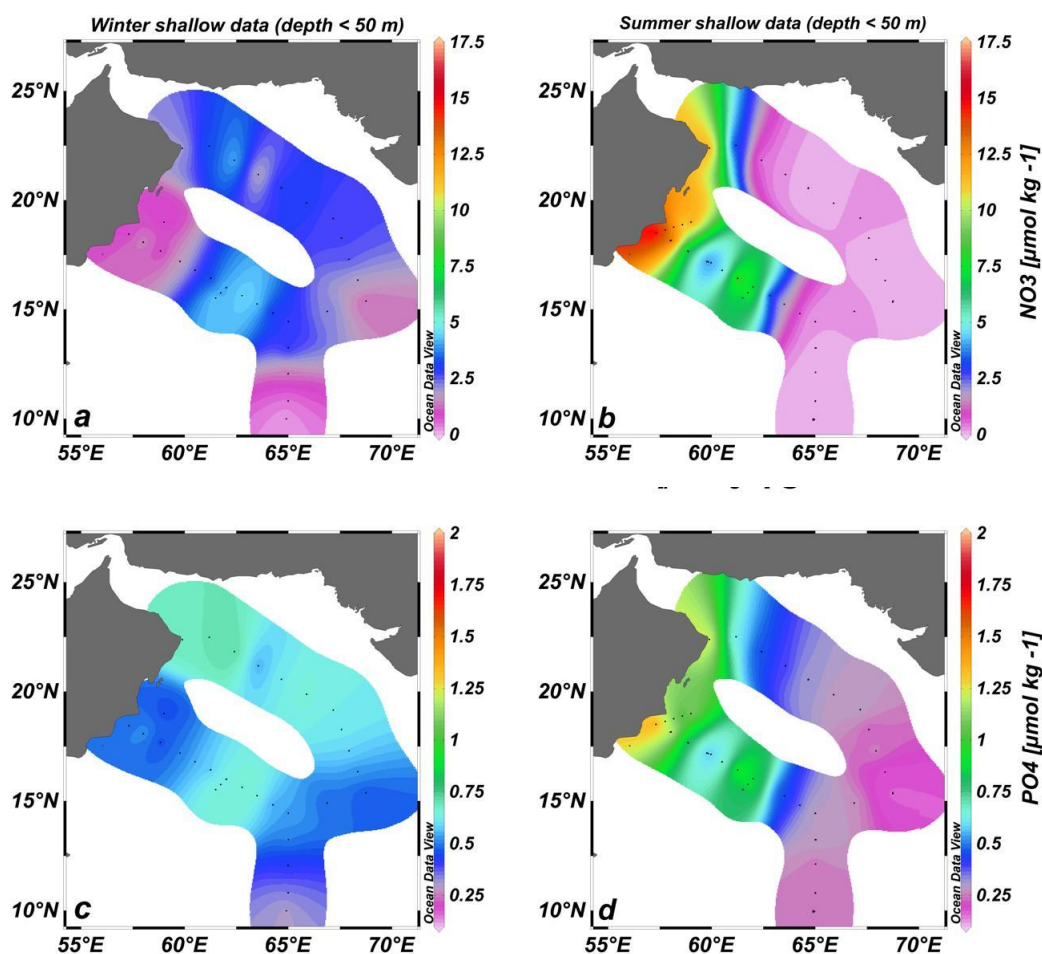


FIGURE 2.10: Seasonal variability of nutrients in the upper 50 m in the Arabian Sea. Winter distribution (a) and (c), summer distribution (b) and (d) of nitrate and phosphate, respectively. Data from JGFOS cruises, 1995 (see Chapter 5).

The vertical profiles of nitrate are shown in Figure 2.11. In general, lower concentrations are seen at intermediate depths at the northern latitudes compared to southern latitudes as was also reported by DeSousa et al. (1996).

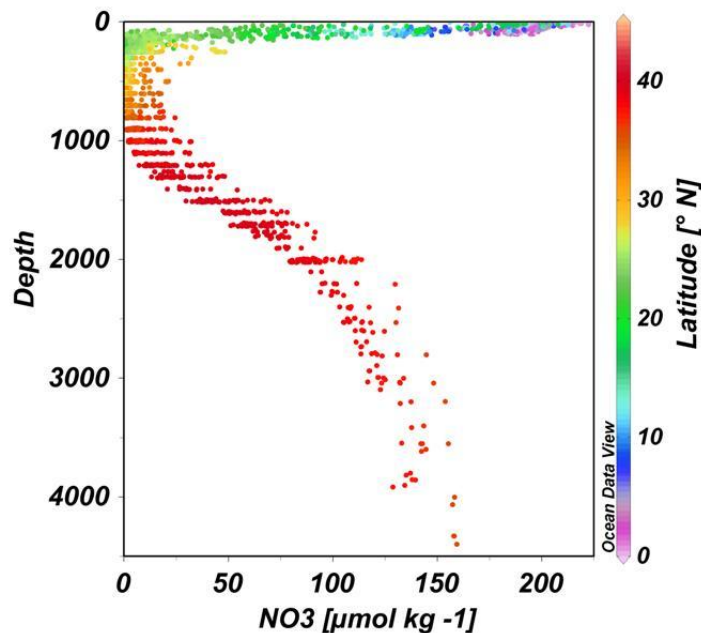


FIGURE 2.11: NO_3 profiles in the Arabian Sea, data from JGOFS 1995 (see chapter 5).

2.2 Red Sea

The Red Sea is located between the Mediterranean Sea and the Indian Ocean and is bordered by Egypt, Sudan, Eritrea, and Djibouti on the western side, and Yemen and Saudi Arabia on the eastern side (Figure 2.12). The Red Sea is a relatively newly formed ocean located in an arid zone between 12.5°N and 30°N . It is a deep trench resulting from a separation of the Arabian plate from the African plate. At the southern end of the Red Sea is the strait of Bab el Mandeb (literally "Gate of Lamentations"), only 29 km wide and with a maximum depth of 130 m. The strait of Bab el Mandeb is the only connection between the Red Sea and the Gulf of Aden and Indian Ocean.



FIGURE 2.12: Map of the Red Sea and the Gulf of Aden. Also shown are the states bordering the Red Sea.

There is a net flow of water from the Gulf of Aden to the Red Sea to compensate for evaporative losses. Restricted exchange with the open ocean results in saline water with high density and low oxygen concentrations due to respiration/remineralization. The Red Sea high saline water is one of the warm deep water formation sites in the world. The bathymetry of the Red Sea region is shown in Figure 2.13 and basic information can be found in Table 2.2. The widest point is found near Massawa (Eritrea) and is about 300 km. The average depth is about 500 m but its greatest depth exceeds 2000 m.

The Red Sea splits into two branches in the north; these are Gulf of Aqaba to the northeast and Gulf of Suez to the northwest. Gulf of Aqaba is short and narrow, 150 km by 16 km, but also deep, up to 1800 m. The Strait of Tiran, with a sill depth of 250–300 m, separates the Gulf of Aqaba and the Red Sea. The Gulf of Suez has a length of 280 km and a width of 20–40 km, and is currently spreading due to normal faulting. It is very shallow with depths mostly ranging from 55–73 m, reaching nearly 100 m at the southern end where it meets the Red Sea. In contrast to the Gulf of Aqaba, the sea-floor of the Gulf of Suez is generally flat (Bonfil and Abdallah, 2004).

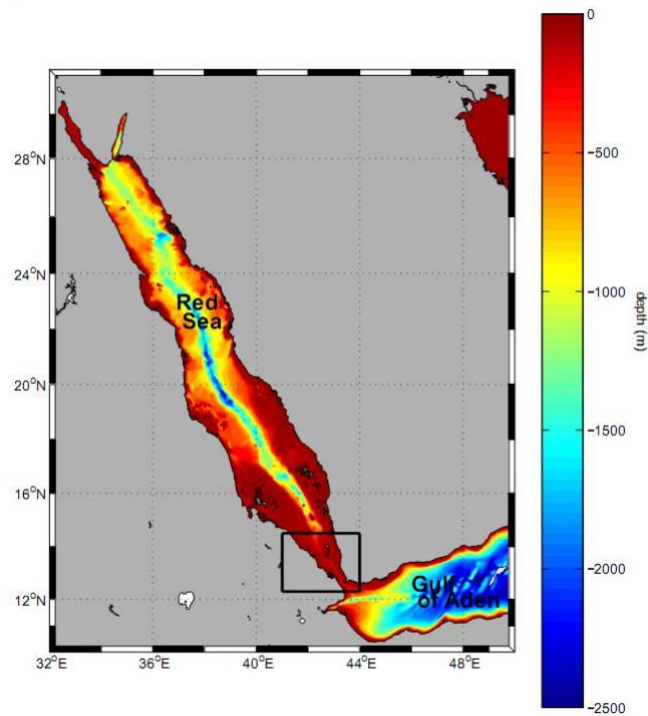


FIGURE 2.13: General bathymetry of the Red Sea and Gulf of Aden.

TABLE 2.2: Basic information of the Red Sea region, modified from Ali (2008).

Area	Parameter	Magnitude	Reference
Red Sea	Surface area	458620 km ²	Sea Around Us (2007)
	Average depth	500 m	Patzert (1974)
	Length	1930 km	Patzert (1974)
	Maximum depth	2920 m	Morcos (1970)
	Average width	220 km	Patzert (1974)
Gulf of Aqaba	Length	150 km	Bonfil and Abdallah (2004)
	Depths range	1100-1400 m	Edwards (1987)
	Width	16 km	Bonfil and Abdallah (2004)
Gulf of Suez	Length	280 km	Bonfil and Abdallah (2004)
	Depths range	55-73 m	Bonfil and Abdallah (2004)
	Width range	20-40 km	Bonfil and Abdallah (2004)
Strait of Bab el Mandeb	Narrowest width	18 km	Murray and Johns (1997)
	Sill depth	137 m	Werner and Lange (1975)

2.2.1 Hydrographic condition

The Red Sea is located in an arid region with extremely hot weather in the summer. The southern region is considered to be among the hottest regions in the world.

Rainfall in the Red Sea region is extremely sparse and amounts annually to around 110 mm (PERSGA, 2004). The currents in the Red Sea are largely driven by density gradients in the water column and winds. The main current feature in the south is located between 15°N and 16°N which reverses from an anticyclonic rotation during winter to a cyclonic rotation during the summer (Figure 2.14). The mean meridional transport at the surface is during winter directed predominantly to the north and at each side a boundary current exists, flowing northwards. During summer, when the direction of the winds over the southern Red Sea and the Gulf of Aden is reversed, the northward western boundary current disappears in the southern part of the Red Sea and the surface flow reverses.

During transition periods, currents are weakest and most variable. In all seasons, hydrographic observations and velocity measurements show that surface circulation consists of a series of cyclonic and anticyclonic gyres that disappear and reappear at preferential locations (Morcos and Soliman, 1974; Woelk and Quadfasel, 1996) as a consequence of the wind field which is steered by the adjacent topography. Thus, density forcing and wind interact at different times and places to generate a rather complex surface circulation pattern (Sofianos and Johns, 2003).

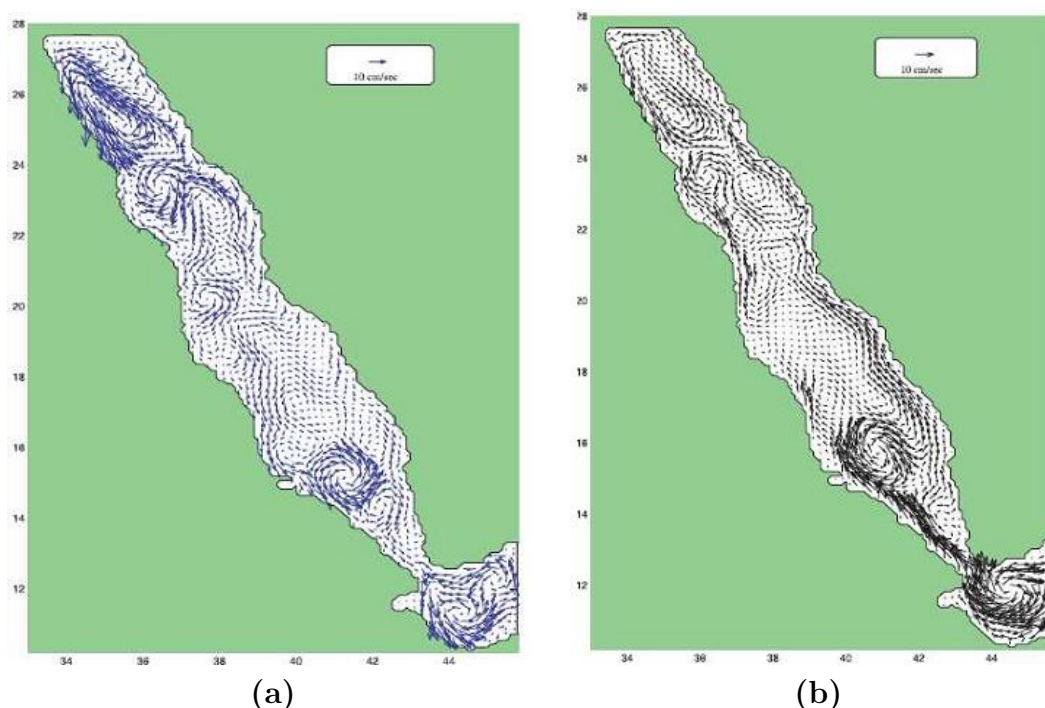


FIGURE 2.14: The mean surface circulation in the Red Sea during (a) winter and (b) summer, from MICOM simulation (Sofianos and Johns, 2003).

During winter the strong south-southeasterly winds present in the southern Red Sea cause a large surface inflow from the Indian Ocean (Figure 2.15) while during summer water from the Red Sea is found at the surface, flowing south. At intermediate depth, the fresher and colder Gulf of Aden Intermediate Water flows northward over the sill in summer but not during winter (Al Saafani and Shenoi, 2004). In both seasons the Red Sea Overflow Water (RSOW) leaves the Red Sea over the sill.

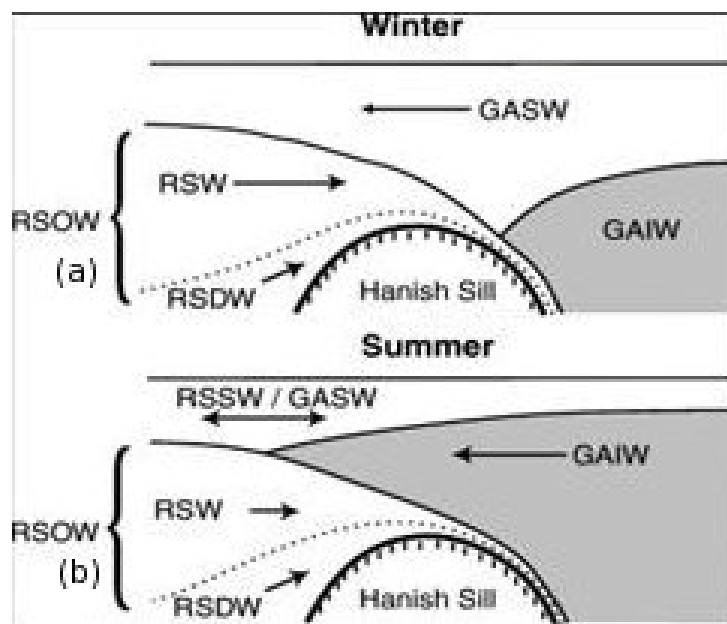


FIGURE 2.15: Schematic of the (a) winter and (b) summer water exchange regimes in the strait of Bab el Mandeb, where GASW is Gulf of Aden Surface Water, RSW is Red Sea Surface Water, GAIW is Gulf of Aden Intermediate Water, RSDW is Red Sea Deep Water, and RSOW is Red Sea Overflow Water (from Siddall et al., 2002).

The Red Sea experiences surface temperatures of over 32°C during summer and rarely colder than 20°C during winter. The temperature pattern is complicated, with its maximum at the center of the basin and decreasing temperatures towards the two ends of the Red Sea. The decrease of surface temperature towards the Bab el Mandeb is due to the influx of colder water from the Gulf of Aden (Rohling and Zachariasse, 1996; Sofianos and Johns, 2003), while the decrease in the north is due to the high evaporation developed in this region (Goyet et al., 1999). The deeper waters are stable throughout the region, and below 300 m the water temperature is constantly between 21 and 22°C (Figure 2.16).

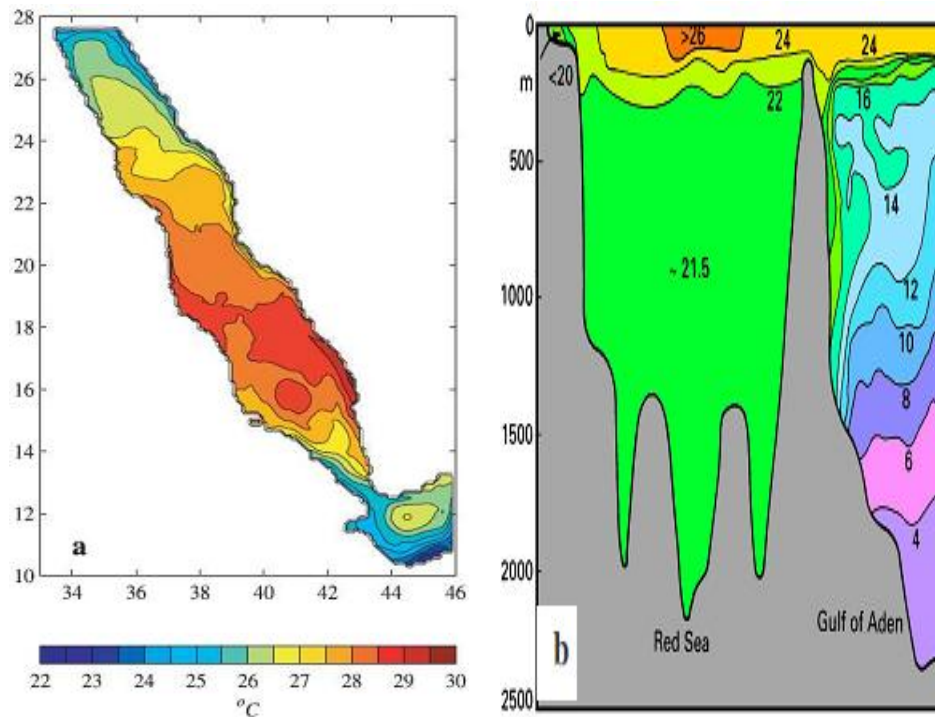


FIGURE 2.16: Distribution of potential temperature ($^{\circ}\text{C}$) in the Red Sea (a) surface and (b) water column (from Sofianos and Johns, 2003).

The surface salinity in the Red Sea is generally high within the range 36-46 (Sofianos and Johns, 2003) due to high evaporation, low precipitation, and the lack of a major river inflow (Figure 2.17 a). Salinity is usually lower in the southern region due to the inflowing waters from the Gulf of Aden and it increases northwards due to evaporation. The evaporation levels of 1 to 2 m yr^{-1} greatly exceed precipitation (10 mm yr^{-1}) in this area. In addition, the salinity increase with latitude is higher in summer than in winter. Salinity increases with depth (Figure 2.17b) and the bottom of the halocline is marked by the 40.5 isohaline. The vertical gradient in the pycnocline is very strong in the south and decreases gradually towards the north. In the north the vertical gradients of temperature and salinity are much smaller in winter and deep water appears to be better mixed than in the summer. Below 200 m the deep basin of the Red Sea is filled with waters of extremely homogeneous salinity of about 40.6.

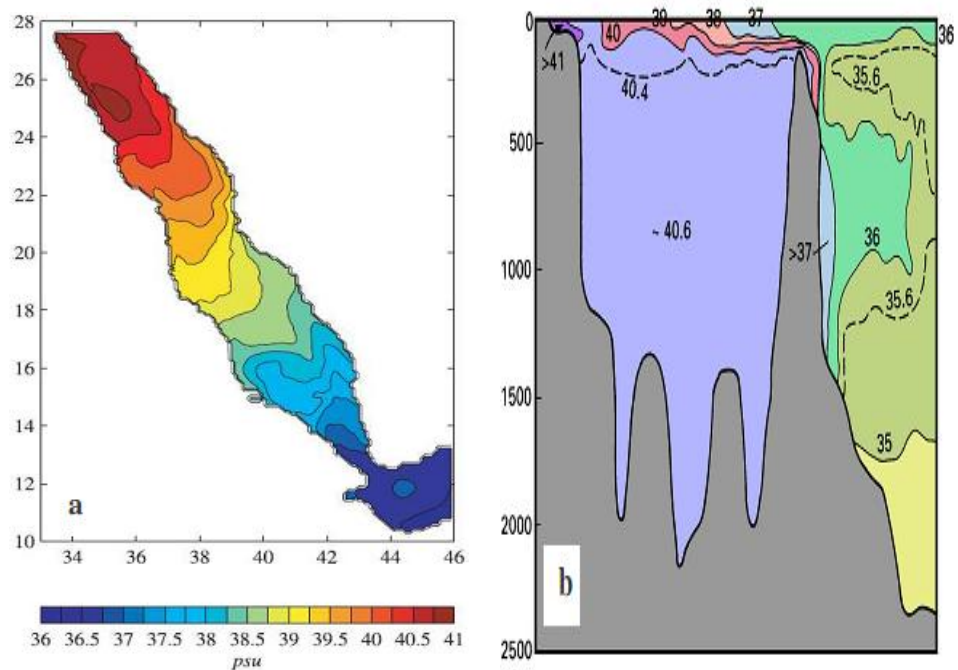


FIGURE 2.17: Salinity distribution in the Red Sea (a) surface water and (b) water column (from Sofianos and Johns, 2003; Tomczak and Godfrey, 2001).

In the northern Red Sea and Gulf of Suez, the dens saline surface water cools during winter, sinks below the thermocline, and flows southwards and into the Gulf of Aden. The water mass exchange between these two layers is limited to winter deep convection at the northern end and upwelling over the whole area (Figure 2.18). A free communication between the deep water of the Indian Ocean and the Red Sea is prevented by the shallow Hanish Sill with about 137 m depth just north of Bab el Mandeb.

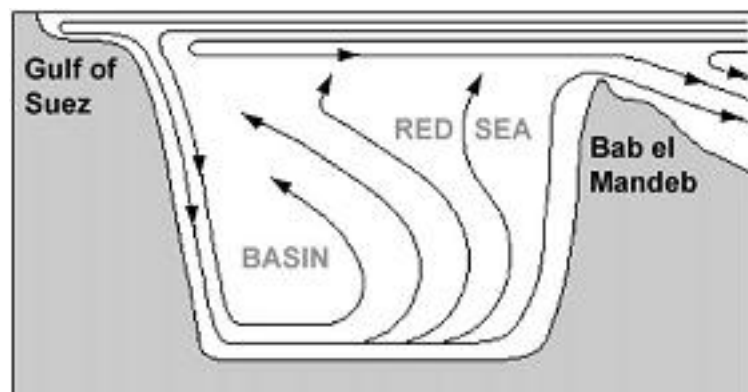


FIGURE 2.18: Sketch of the Red Sea circulation (Jean-Baptiste et al., 2004).

Some small, enclosed basins exist within the central Red Sea where pockets of very dense, saline, hot water are found. The salt content of these brine pools is greater than 25% by weight compared to normal Red Sea salinity of about 4%. Temperatures of the hot brines can exceed 50°C. The density contrast between the hot brines and the overlying seawater is great enough to cause a reflection of the sound waves used by echo sounders. The hot water result from hydrothermal circulation through the highly fractured, young oceanic crust, while the salt comes from the thick layer of evaporates. The hydrothermal circulation, in addition to heating the water, results in leaching of heavy minerals from the igneous rocks of the upper crust. These minerals become concentrated in the brine pools and precipitate out, resulting in the formation of sediments with very high concentrations of iron, manganese, zinc, lead, copper, and silver. Various schemes have been proposed to exploit these mineral deposits, but none have proved feasible ([Anschutz and Blanc, 1996](#)).

2.2.2 Chemical and biological conditions

The horizontal and vertical dissolved oxygen distribution in the Red Sea is mainly dominated by water temperature and salinity through solubility ([Rasheed et al., 2002](#)). Surface water is close to saturation with respect to dissolved oxygen. During the winter season, the concentration of dissolved oxygen at the surface ranges from about 4.4 to 4.9 ml l⁻¹ (refers to 192–213 μmol kg⁻¹). Higher values are generally found in the northern and southern Red Sea due to the low water temperature in the north and to the intensive photosynthesis in the south while minimum concentrations of dissolved oxygen are found in the central Red Sea (19°–20°N) along with high sea surface temperatures (Figure 2.19). The summer concentration of dissolved oxygen at the surface is lower than in winter which falls in the ranges of 3.8–4.6 ml l⁻¹ (refers to 165–200 μmol kg⁻¹), due to the higher temperature and salinity of the surface water ([Douabul and Haddad, 1999](#)).

The vertical distribution of dissolved oxygen in the Red Sea can be divided into three layers:

1. A surface layer with high oxygen content ($3.5\text{--}4.9\text{ ml l}^{-1}$) that extends from the surface to a depth of 50–180 m, being shallower near the sill and is deeper in winter than in summer.
2. An intermediate layer in which the oxygen content decreases rapidly with depth to reach a minimum at about 400–600 m.
3. A deep layer in which oxygen content is substantially higher than the intermediate layer.

There is a rapid decrease of dissolved oxygen in subsurface layer in the southern Red Sea, particularly near the sill of Bab el Mandeb at depths between 40 and 130 m. This is attributed to the subsurface inflow of high nutrient, low oxygen Gulf of Aden upwelled water (Douabul and Haddad, 1999).

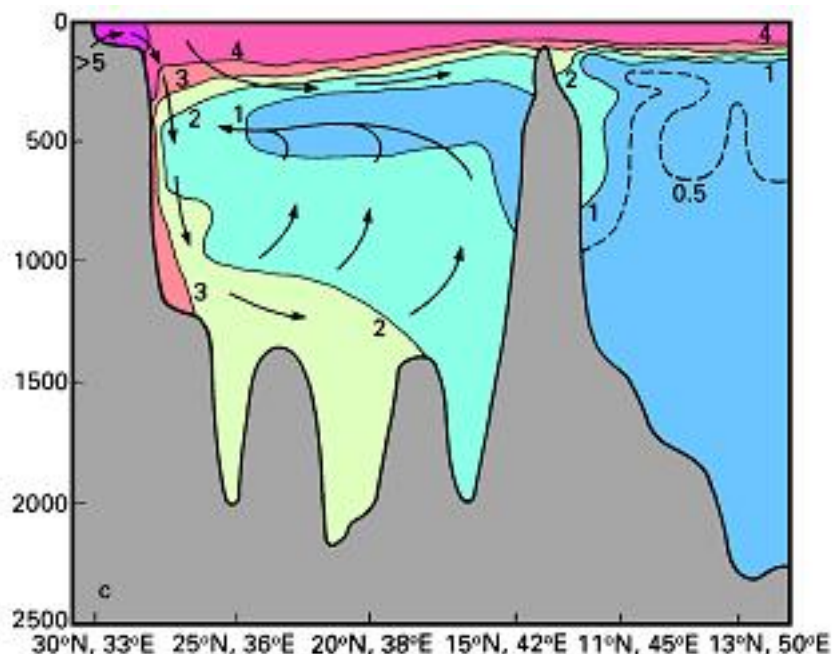


FIGURE 2.19: Hydrographic section of oxygen (ml l^{-1}) in the Red Sea during winter (1 ml l^{-1} is equivalent to about $43.6\ \mu\text{mol kg}^{-1}$, assuming a density of 1.025 kg l^{-1}).

Nutrients, such as nitrate, phosphate, ammonium, and silicate are essential for phytoplankton growth. Generally, the Red Sea surface waters are exceptionally oligotrophic (clear and low in nutrients) especially in the open waters, compared to the Gulf of Aden, and this is due to the hot, arid climate, rare runoff, low

rainfall, and little nutrient input from soil. However, nutrients distribution denotes remarkable variations with depth and by season from north to south. Nutrient concentrations throughout the water column in the southern Red Sea are higher than those in the central and northern region because the southern part of the Red Sea is affected by the inflow of rich intermediate water from the Gulf of Aden during late summer (Douabul and Haddad, 1999).

The Red Sea has an extraordinary range of biological diversity and it is an important repository of marine biodiversity (Hasan, 2009; Perrings, 2009). Its relative isolation has given rise to particular coral reef systems which comprise more than 250 species of scleractinian corals, representing the highest diversity in any section of the Indian Ocean. The northern coasts of the Red Sea and the Gulf of Aqaba have an almost continuous band of coral reef, which physically protects the shoreline (Figure 2.20). Coral assemblages in the shallow Gulf of Suez are less well developed. Further south the shelf becomes much broader and shallower and the fringing reefs gradually disappear (Bonfil and Abdallah, 2004).



FIGURE 2.20: Map of the Red Sea coral reef distribution (from Kotb et al., 2004).

Ocean carbon cycle

The global carbon cycle involves the earth's atmosphere, fossil fuels, the oceans, and the vegetation and soils of the earth's terrestrial ecosystems (Post et al., 1990). The ocean has the largest carbon storage capacity amongst the carbon reservoirs on earth (Figure 3.1).

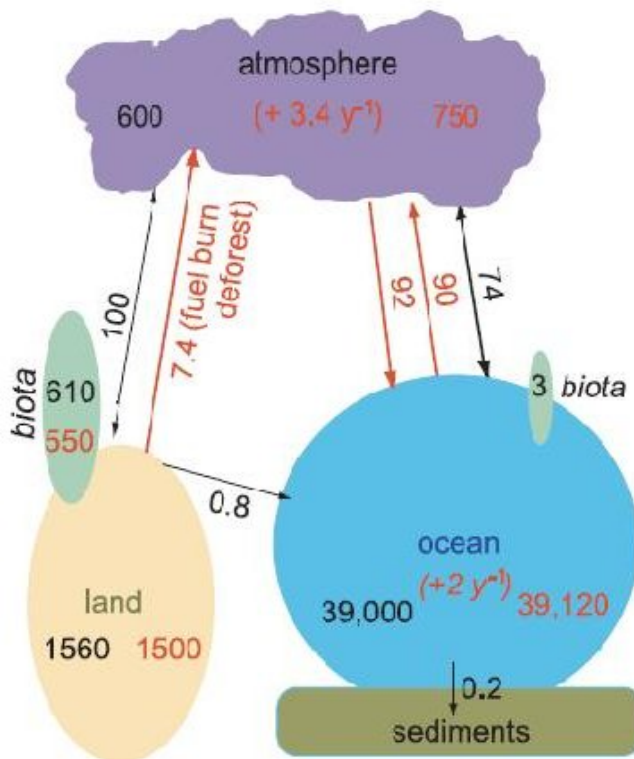
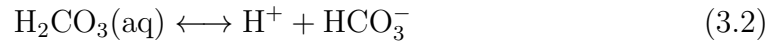
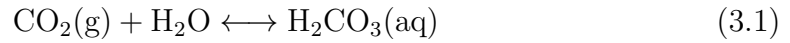


FIGURE 3.1: Global carbon cycle. Numbers in black are preindustrial and red are those influenced by human activities. Numbers inside the earth compartments are the respective reservoir sizes and those next to arrows are rates of carbon transfer. Black arrows indicate estimated rates for preindustrial era whereas red arrows account for anthropogenically modified rates. Red numbers within brackets are the accumulation rates of anthropogenic carbon dioxide in atmosphere and oceans in Gt y^{-1} ($\text{Gt C} = 10^{15} \text{ g C}$) (from <http://www.whrc.org/carbon/index.htm>).

Carbon chemistry is therefore important in understanding the ocean carbon system. There are four essential parameters that can be measured to obtain a complete description of the carbon system in seawater. These are total dissolved inorganic carbon (DIC), total alkalinity (TA), fugacity of carbon ($f\text{CO}_2$), and pH (Dickson and Goyet, 1994).

DIC: When carbon dioxide (CO_2) enters the ocean it reacts with seawater and forms carbonic acid (H_2CO_3). Then carbonic acid is further dissociated in two steps and forms bicarbonate ions (HCO_3^-) and carbonate ions (CO_3^{2-}) according to the following equations:



The total dissolved inorganic carbon in a seawater sample is the sum of the dissolved carbon forms i.e. CO_2 , HCO_3^- and CO_3^{2-} :

$$\text{DIC} = \text{CO}_2 + \text{HCO}_3^- + \text{CO}_3^{2-} \quad (3.4)$$

TA: The total alkalinity of a seawater sample is defined as the number of moles of hydrogen ion equivalent to the excess of proton acceptors over proton donors in one kilogram of sample (Dickson and Goyet, 1994). TA includes the species that neutralize hydrogen ions, minus the offsetting effect of hydrogen ions present in the solution:

$$\begin{aligned} \text{TA} = & [\text{HCO}_3^-] + 2 [\text{CO}_3^{2-}] + [\text{B}[\text{OH}]_4^-] + [\text{OH}^-] + [\text{HPO}_4^{2-}] + 2 [\text{PO}_4^{3-}] + \\ & [\text{SiO}[\text{OH}]_3^-] + [\text{NH}_3] + [\text{HS}^-] - [\text{H}^+]_F - [\text{HSO}_4^-] - [\text{HF}] - [\text{H}_3\text{PO}_4] \quad (3.5) \end{aligned}$$

The minor acid or base species in equation 3.5 occur in such small amounts that they can be neglected. The most important part of the total alkalinity in the

seawater is defined as:

$$\text{TA} = [\text{HCO}_3^-] + 2 [\text{CO}_3^{2-}] + [\text{B}[\text{OH}]_4^-] + [\text{OH}^-] - [\text{H}^+]_F \quad (3.6)$$

where $[\text{H}^+]_F$ is the free concentration of hydrogen ion.

$f\text{CO}_2$: The fugacity of carbon dioxide is relatively similar to the partial pressure of CO_2 (pCO_2). pCO_2 is defined as the partial pressure of CO_2 in a small air volume in equilibrium with the water phase;

$$\text{pCO}_2 = \frac{[\text{CO}_2]}{K_0} \quad (3.7)$$

where K_0 is the gas solubility. $f\text{CO}_2$ differs from pCO_2 in that it takes account of the non-ideal nature of the gas phase (Dickson and Goyet, 1994). $f\text{CO}_2$ can be determined from knowledge of its equation of state:

$$f\text{CO}_2 = \text{pCO}_2 \exp\left(\frac{P(B + 2\delta)}{RT}\right) \quad (3.8)$$

where $f\text{CO}_2$ and pCO_2 are in μatm , P is the total atmospheric pressure in Pa (1 atm = 101325 Pa), B is the first virial coefficient of CO_2 , and δ is the cross virial coefficient, both are in $\text{m}^3 \text{mol}^{-1}$. R is the gas constant and is equal to $8.314 \text{ J K}^{-1} \text{ mol}^{-1}$, and T is the absolute temperature in Kelvin. B has been determined by Weiss (1974):

$$B = (-1636.75 + 12.0408T - 3.27957 \times 10^{-2}T^2 + 3.16528 \times 10^{-5}T^3) 10^{-6} \quad (3.9)$$

and δ is given by:

$$\delta = (57.7 - 0.118T) 10^{-6} \quad (3.10)$$

pH: pH is defined as the negative logarithm of hydrogen ions concentration in gram atoms per liter:

$$\text{pH} = -\log [\text{H}^+] \quad (3.11)$$

The pH of the ocean ranges between 1 and 14. It can be considered to be an

intensity factor which measures the concentration of alkali or acids immediately available for reaction, while the alkalinity is a capacity factor which is a measure of the ability of a water sample to stay unchanged when acids are added. In seawater, the pH is generally around 8 and is controlled by the relative amounts of the different ion concentrations ($[\text{HCO}_3^-]$, $[\text{CO}_3^{2-}]$, $[\text{OH}^-]$, $[\text{H}^+]$, etc.), see Figure 3.2. If two of the parameters (DIC, TA, pCO_2 , and pH) and the equilibrium constants of the system are known the other two variables can be calculated (Dickson and Goyet, 1994; Zeebe and Wolf-Gladrow, 2001).

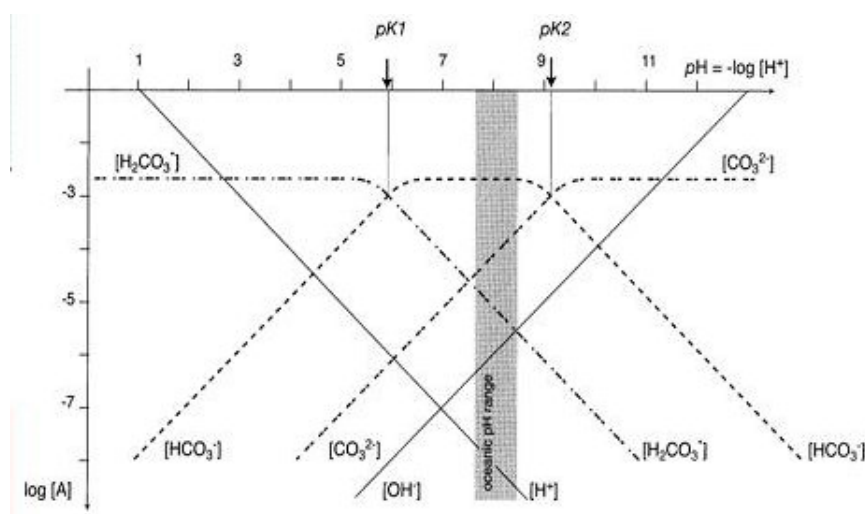


FIGURE 3.2: Concentrations of the different inorganic carbon species as a function of pH. Equilibrium constants for equations 3.2 and 3.3 are indicated in the figure (from Sarmiento and Gruber, 2006).

To understand the fate of CO_2 in the ocean, we must understand the mechanisms that control the carbon cycle. These are the solubility pump and the biological pump (Figure 3.3).

The solubility pump depends on temperature and salinity (Gordon and Jones, 1973; ?). Cold water holds more gas than warm water, and carbon dioxide that dissolves into cold ocean water at high latitudes is carried to the deep ocean by sinking currents, where it stays for hundreds of years. Eventually, mixing brings the water back to the surface and the ocean emits CO_2 into the tropical atmosphere (Figure 3.4). This marine physical carbon pump transports carbon from the atmosphere into the sea for long term storage.

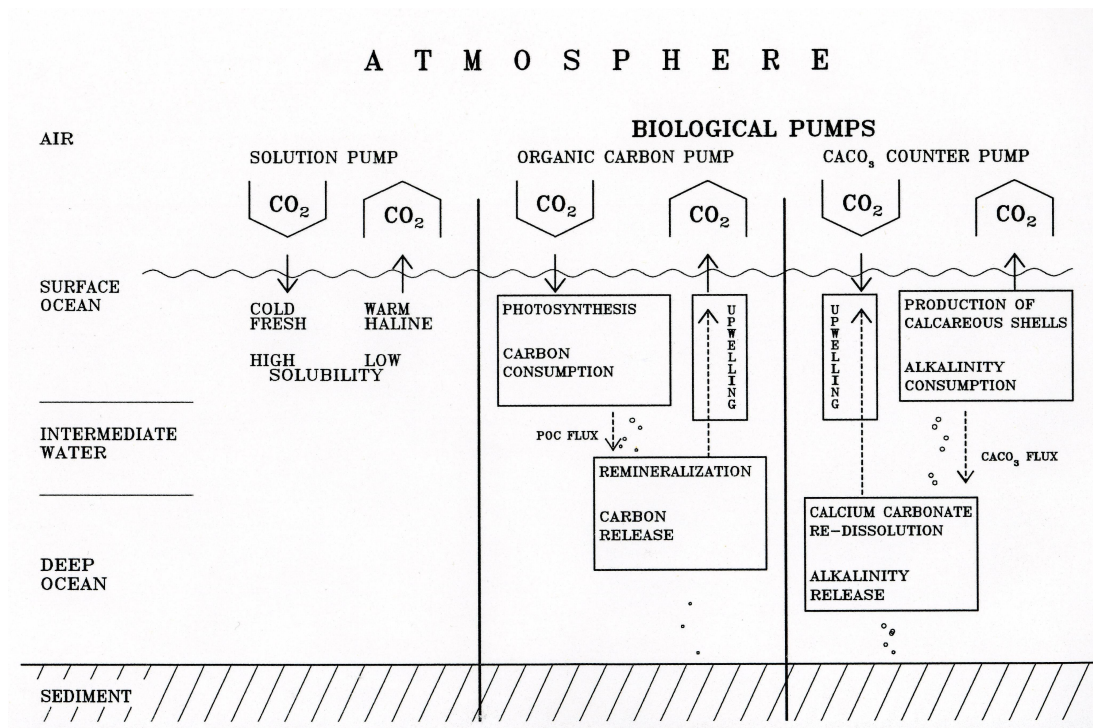


FIGURE 3.3: A sketch showing different pumps transporting CO_2 between atmosphere and ocean, and also within the ocean (from Heinze et al., 1991).

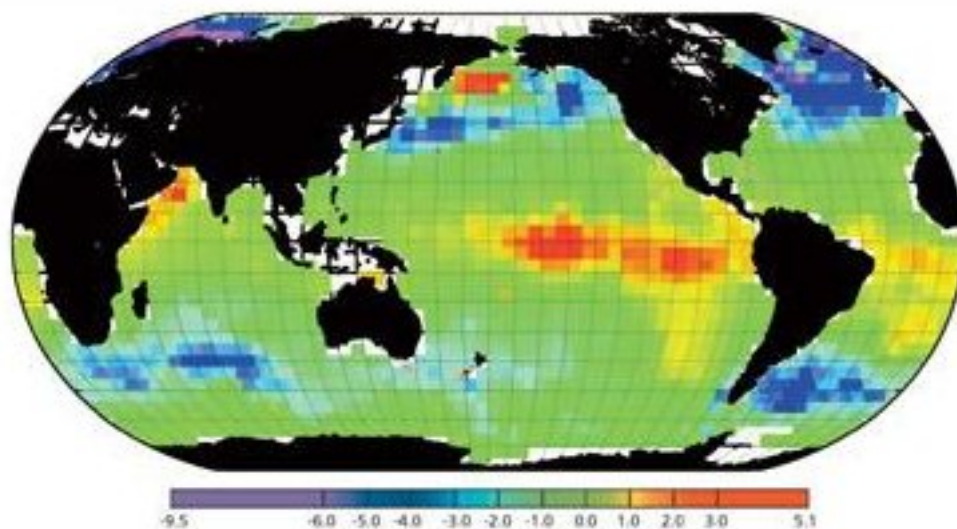


FIGURE 3.4: Global map of the average annual exchange of CO_2 ($\text{mol C m}^{-2} \text{ y}^{-1}$) across the sea surface (from <http://oceanworld.tamu.edu/resources/oceanography-book/carboncycle.htm>).

The biological pump describes exchange of carbon between the atmosphere and the sea through biological fixation of carbon and transport of carbon from the surface euphotic zone to the ocean's interior. The biological pump includes two types of carbon pumps, the organic carbon pump and the calcium carbonate pump (Figure 3.3). The organic carbon pump describes a process where phytoplankton use CO_2 during photosynthesis and produce organic matter and oxygen. When phytoplankton and animals die they sink deeper into the ocean. These organic materials are called reduced carbon and most of the reduced carbon is used by animals and bacteria and can be remineralized to energy, water, and CO_2 . Eventually, a small fraction of the reduced carbon (0.4%) is buried and stored in sediments for millions of years and introduced into the surface again by upwelling of the deep water. The calcium carbonate pump releases CO_2 and consumes TA (Figure 3.3) through the production of carbonate skeletons and shells (particulate inorganic carbon, PIC). Most of the PIC is in the form of calcite and aragonite. The two types of biological carbon pumps have different effects on the seawater's carbonate system. In the surface ocean, the organic carbon pump reduces pCO_2 , whereas the calcium carbonate pump increased pCO_2 . In the deep ocean, a part of the organic carbon becomes oxidized, increasing CO_2 (respired CO_2), but the dissolution of calcium carbonate consumes CO_2 (Zhifei et al., 2003).

Processes controlling alkalinity

The TA varies in the ocean both horizontally, vertically, and with season. The TA distributions are primarily controlled by physical factors such as weathering, temperature, and salinity, and biological factors, such as production/precipitation/dissolution of calcium carbonate, organic carbon production through nitrate uptake, or remineralization. The alteration in TA can also be a result of uptake/release of protons associated with reduction/oxidation of some nutrients but this is negligible in the open-ocean variability of TA (Sabine et al., 2002). Figure 4.1 shows the different processes controlling TA and DIC. During calcium carbonate formation both TA and DIC decrease, while during photosynthesis TA increases and DIC decreases. Air-sea gas exchange only affects the DIC of the water.

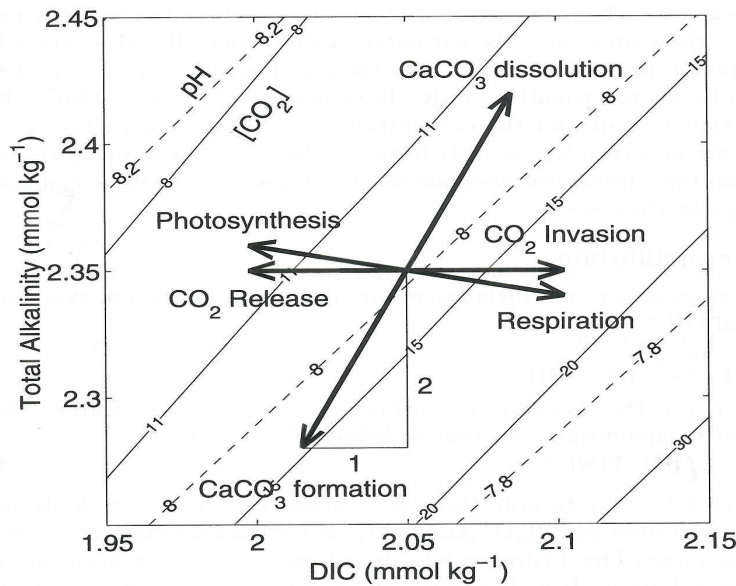


FIGURE 4.1: A sketch showing how different processes affect DIC and TA. TA varies mainly with formation and dissolution of calcium carbonate (from Zeebe and Wolf-Gladrow, 2001).

4.1 Alkalinity changes due to physical processes

The main physical processes that control TA are salinity and weathering. Weathering of land, rocks of carbonate and silicate, hydrothermal activity, and reverse weathering are sources and sinks of TA in the ocean. Recently, it has been demonstrated that the weathering has a significant role in the global carbon cycle since the silicate rock weathering followed by the formation of carbonate rocks in the ocean transfers CO₂ from the atmosphere to the lithosphere (Background, 2007; Galy and France-Lanord, 1999; Sigman and Boyle, 2000). Weathering will not be further explored in this thesis.

The distribution of TA in the open ocean is primarily a conservative function of salinity, and those physical factors that regulate salinity (e.g. water mass movements, mixing, evaporation, and dilution due to freshwater addition by sea ice melt, river runoff, and precipitation). Surface TA variations associated with changes in salinity account for more than 80% of total variability in TA (Lee et al., 2006). Such strong salinity-dependent trends in surface TA result from the fact that the concentrations of the key chemical species (i.e. HCO₃⁻, CO₃²⁻, and B(OH)⁴⁻) that contribute to TA increase proportionally with increasing salinity.

At higher latitudes, north of 30° N or south of 30° S, precipitation exceeds evaporation and thus salinity decreases with latitude. Convective mixing of deep water occurs with seasonal cooling and is an important additional factor that acts to increase surface TA concentrations. This is because vertical mixing brings deep waters rich in CaCO₃ to the surface. As a result, the values of TA generally decrease (Figure 4.2) with increasing latitude (Lee et al., 2006). Seasonal variations in total alkalinity are directly proportional to salinity and generally larger in the subtropics than in the higher-latitude oceans. In particular, larger amplitudes of the seasonal variability are observed in areas where freshwater inputs through rivers and the ice melting or where tropical upwelling occurs (Lee et al., 2006).

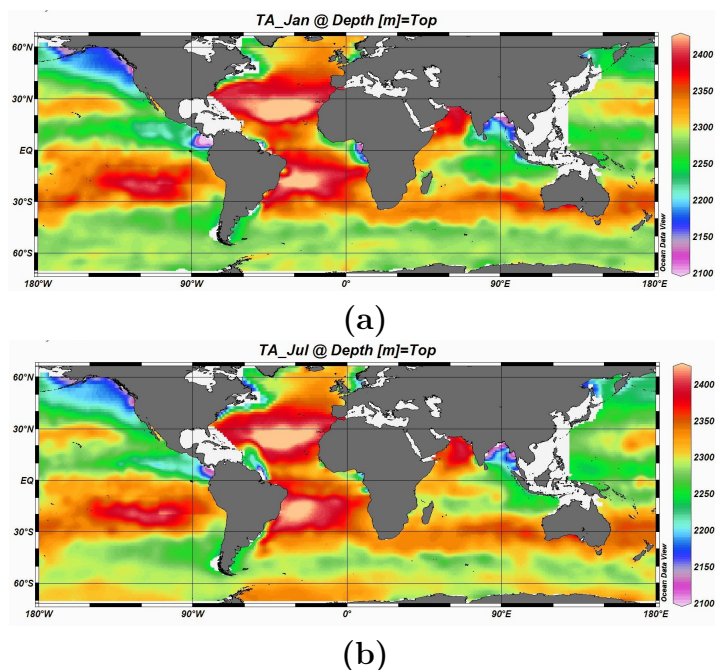


FIGURE 4.2: Monthly mean values of surface TA ($\mu\text{mol kg}^{-1}$) for (a) January and (b) July for the world's ocean, as estimated from http://cdiac.ornl.gov/oceans/SurfaceAlkalinityClimatology_ODV/Climatology_ODV.html

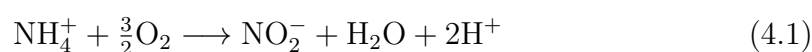
4.2 Alkalinity changes due to biogeochemical processes

Further important changes in TA are due to various biogeochemical processes such as calcium carbonate precipitation or production of particulate organic matter by microalgae. Minor alteration of TA by the latter two processes is caused by the uptake/release of protons associated with reduction/oxidation of some nutrients associated by other bacterial processes affecting carbonate alkalinity, these are: carbon dioxide formation, sulfate reduction, ammonia formation, and denitrification (Berner et al., 1970; Sabine et al., 2002).

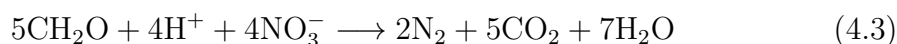
4.2.1 Assimilation and remineralization of nutrients

Nitrogen assimilation, remineralization, nitrification, and denitrification: Marine photoautotrophs can use nitrate (NO_3^-), nitrite (NO_2^-), ammonia

(NH_4^+), or molecular nitrogen (N_2). Assimilation of 1 mole of nitrate leads to an increase of alkalinity by 1 mole, while a decrease of alkalinity by 1 mole occurs when ammonia is used. On the contrary, no change of alkalinity occurs when molecular nitrogen is the N source. Remineralization of particulate organic matter will change TA depending on the form of produced nitrogen. A release of 1 mole of ammonia or nitrate will lead to an increase or decrease, respectively, of TA by 1 mole (Wolf-Gladrow et al., 2007). In an aerobic environment, ammonia is ultimately oxidized to nitrate. Nitrification according to Schlesinger (1997) is expressed as



This leads to a decrease of TA by 2 moles per mole of NH_4^+ used or nitrate released. Nitrogen fixation (dissolved N_2 converts into nitrate) does not change total alkalinity, but after N_2 is transferred to NO_3^- and NH_4^+ (remineralization and nitrification) TA will be affected. Upon release of nitrogen in the form of NH_4^+ , TA increases by 1 mole per mole N. Nitrification (conversion of NH_4^+ to NO_3^-) decreases TA by 2 moles per mole N. Denitrification process can be described by:



and this process leads to an increase of TA by 1 mole per mole of nitrate converted. However, N_2 fixation and denitrification occur in different regions of the world ocean and these processes will affect the spatial distribution of TA.

Phosphate assimilation and remineralization: The assimilation of phosphate has diminutive effect on TA compared to the effect of nitrate uptake, as marine plankton contain C, N, P in the molar ratios of 106:16:1 (Redfield et al., 1963). During remineralization a release of inorganic phosphate leads to a corresponding small decrease of alkalinity.

Sulfate assimilation and remineralization: The assimilation of sulfate into particulate organic matter leads to an increase of TA by 2 moles per mole of sulfate, and an equivalent decrease of TA occurs due liberation of sulfate during

remineralization. In anoxic sediments methane can be oxidized by sulfate reduction:



and during this process TA increases by 2 moles per mole of methane oxidized due to the decrease of total sulfate (Brewer and Goldman, 1976).

4.2.2 Calcium carbonate formation, precipitation, and dissolution

TA is influenced by the formation and dissolution of marine carbonates, including biogenic magnesian calcites (from coralline algae), aragonite (from corals and pteropods), and calcite (from coccolithophorids and foraminifera), see Figure 4.3.

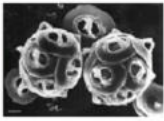



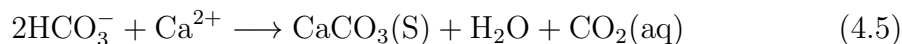
Main calcifying groups		nutrition	mineral form	generation time
Phytoplankton	 Coccolithophores	autotrophic	calcite	day(s)
Zoo-plankton	 Foraminifera	heterotrophic (many with autotrophic symbionts)	calcite	weeks
	 Pteropods	heterotrophic	aragonite	months
	 Corals	heterotrophic (many with autotrophic symbionts)	aragonite	months -years

FIGURE 4.3: The main calcifying groups in the ocean and their generation time.

In the surface ocean, biological production of hard parts, such as shells and skeletons, is the major process leading to CaCO_3 formation (Chierici and Fransson, 2009; Riebesell et al., 2000). The CaCO_3 production varies seasonally and with latitude. Upon formation of calcium carbonate by removal of carbonate or bicarbonate from sea water TA decreases (Bates et al., 1996; Feely et al., 2004;

Iglesias-Rodriguez et al., 2008; Jones and Lu, 2003; Kinsey, 1978) and CO_2 is produced:



Likewise upon death or sinking these calcifying organisms fall through the water column and are either dissolved or deposited in shallow or deep-sea sediments (Archer, 1996; Nozaki and Oba, 1995). The dissolution process is increasing with depth as a function of pressure and adds to the total alkalinity via the reaction:



Aragonite (Ar) and calcite (Ca) are the two most common forms of CaCO_3 found in the ocean. Aragonite is considered as the metastable form and calcite is the stable form which means that aragonite dissolves more easily than calcite due to the different crystalline structure (Figure 4.4). This gives aragonite a shallower horizon (the level at which CaCO_3 is in thermodynamic equilibrium with respect to dissolution) than calcite (Yamanaka and Tajika, 1996).

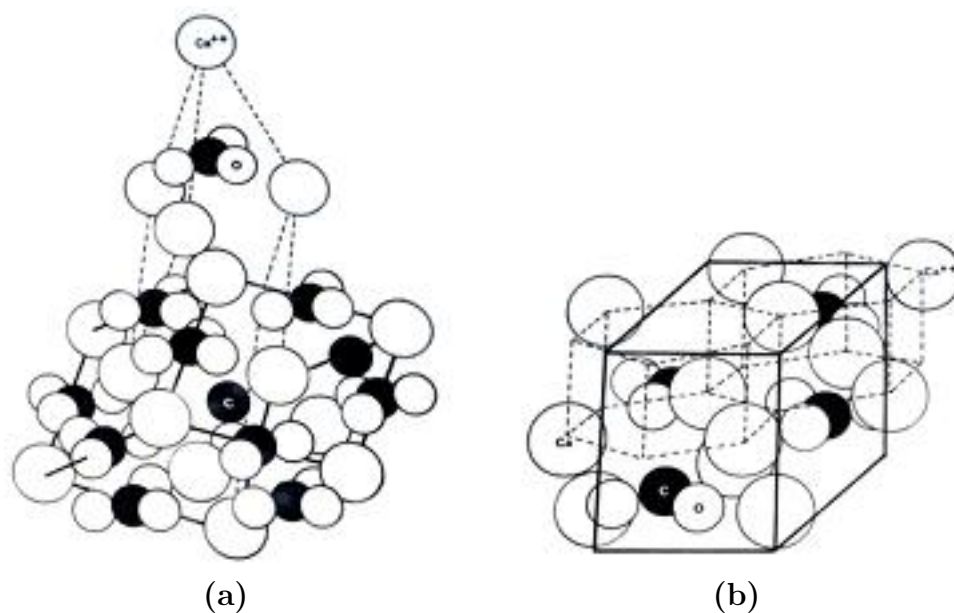


FIGURE 4.4: The crystalline structure of (a) aragonite (Ar) and (b) calcite (Ca).

Calcium carbonate dissolution is one of the important processes that determine carbonate chemistry in ocean. Factors that control this process are: particulate rain rates of calcium carbonate and organic carbon to the deep ocean, saturation of the minerals calcite and aragonite in water overlying sediments, and dissolution of these minerals in undersaturated waters (Emerson and Archer, 1990; Feely et al., 2004; Gangstø et al., 2008). The degree of seawater saturation with respect to calcite and aragonite (Ω_{Ar} or Ω_{Ca}) is defined (at in situ temperature, salinity, and pressure) as:

$$\Omega_{Ar} = \frac{[Ca^{2+}] [CO_3^{2-}]}{K_{spAr}^*} \quad (4.7)$$

$$\Omega_{Ca} = \frac{[Ca^{2+}] [CO_3^{2-}]}{K_{spCa}^*} \quad (4.8)$$

where $[Ca^{2+}]$ and $[CO_3^{2-}]$ denote the seawater concentrations of calcium and carbonate ions, respectively. K_{sp} is the solubility product or stoichiometric solubility constant of calcium carbonate, and can be estimated by:

$$K_{sp}^* = [Ca^{2+}]_{sat} [CO_3^{2-}]_{sat} \quad (4.9)$$

where $[CO_3^{2-}]_{sat}$ and $[Ca^{2+}]_{sat}$ are the concentrations when the equilibrium between $CaCO_3$ and the dissolved ions is achieved, i.e at saturation. If at one location in the ocean the product $[CO_3^{2-}] [Ca^{2+}]$ is higher than K_{sp}^* , the water is said to be supersaturated with respect to $CaCO_3$. If the product is smaller than K_{sp}^* , the water is undersaturated. As the variations of the concentration in Ca^{2+} are much smaller than the variations in the concentration of CO_3^{2-} , saturation is mainly influenced by $[CO_3^{2-}]$.

The degree of saturation does not depend on the carbonate only but also on other factors such as air-sea CO_2 exchange, biological production and respiration, physical mixing, changes in pressure, temperature and salinity as related to freshwater addition. Also cold and fresh water lowers $CaCO_3$ saturation levels as the water dilutes (Chierici and Fransson, 2009). Ocean surface is usually supersaturated with respect to $CaCO_3$ (from Sarmiento and Gruber, 2006) while the deep water usually is undersaturated (Figure 4.5).

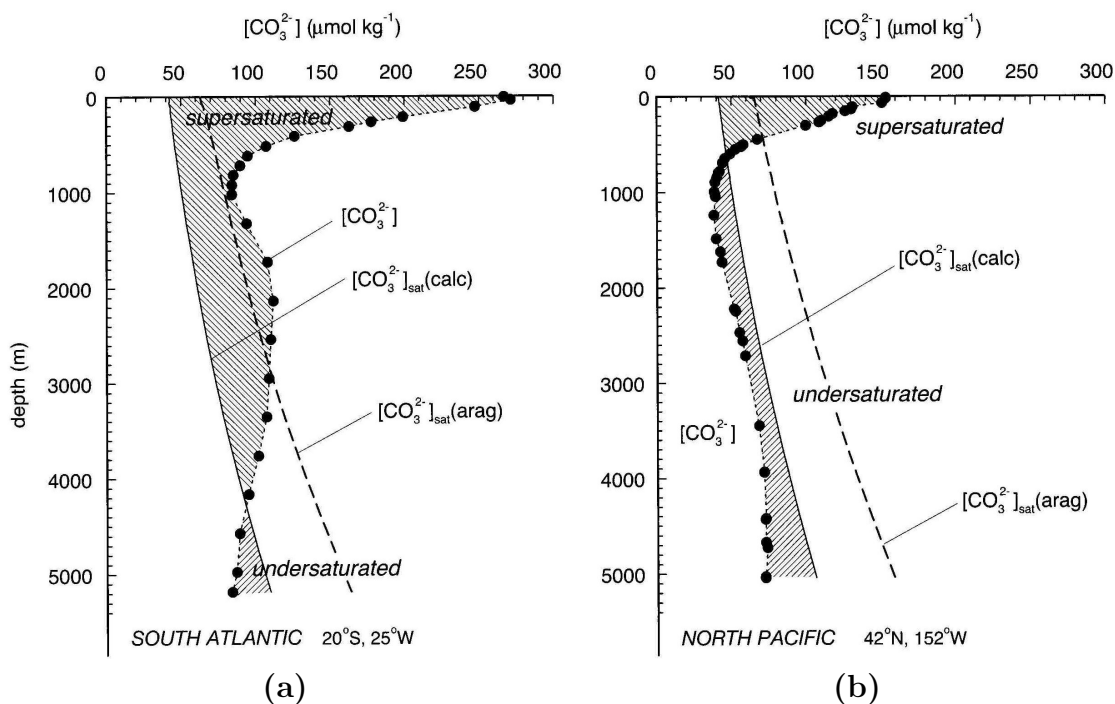


FIGURE 4.5: Carbonate concentrations versus depth and carbonate saturation with respect to aragonite (dashed line) and calcite (solid line) for the south Atlantic (a) and north Pacific (b) (from [Sarmiento and Gruber, 2006](#))

The level at which aragonite and calcite are in thermodynamic equilibrium is known as the saturation depth (Figure 4.6). When the degree of saturation, Ω , is greater than 1, seawater is supersaturated with aragonite and calcite; conversely, seawater is undersaturated with respect to these minerals when $\Omega < 1$. So when the degree of saturation is below one, calcium carbonate, which is generally a stable mineral in present day surface waters, will start to dissolve.

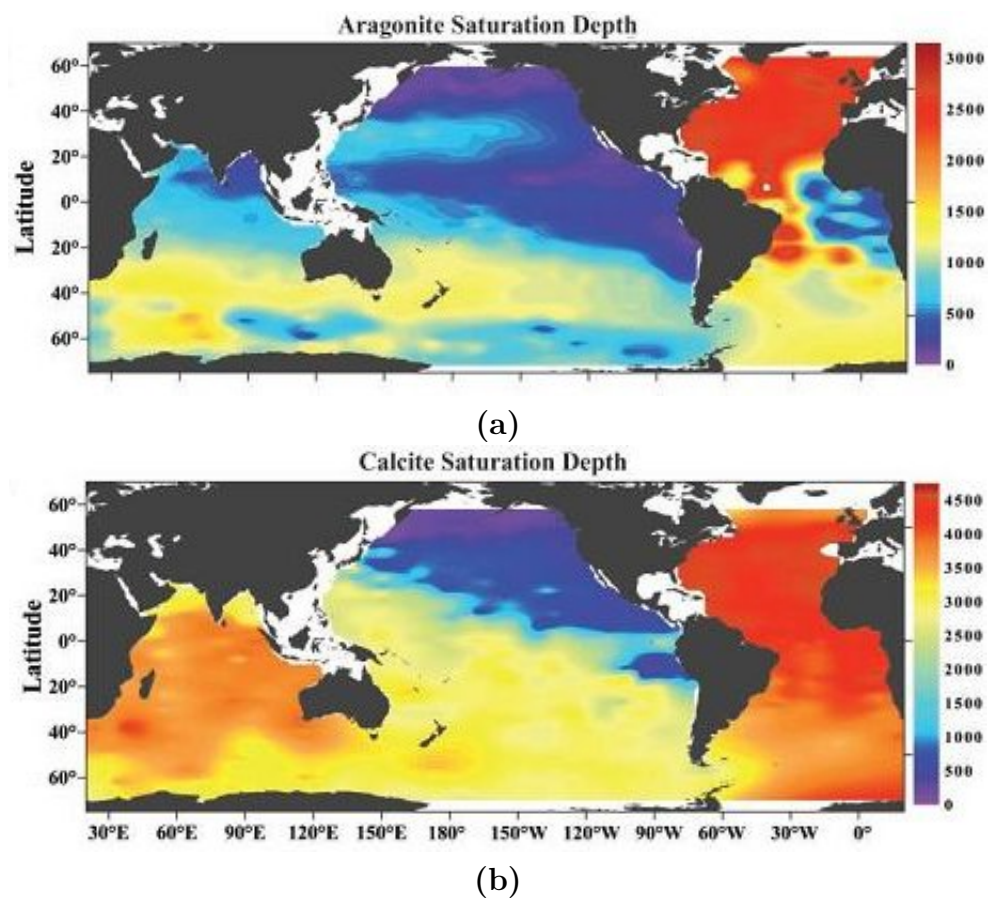


FIGURE 4.6: A global picture of the saturation depth ($\Omega=1$) for (a) aragonite and (b) calcite (from Feely et al., 2004).

Data sets and methodology

5.1 Data sets

We use a combination of data collected during the GEOSECS, MEROU, and JGOFS cruises to investigate the different parameters in the Red Sea and Arabian Sea. GEOSECS 1977 and MEROU 1982 data are from the Red Sea while the JGOFS 1995 data from the Arabian Sea.

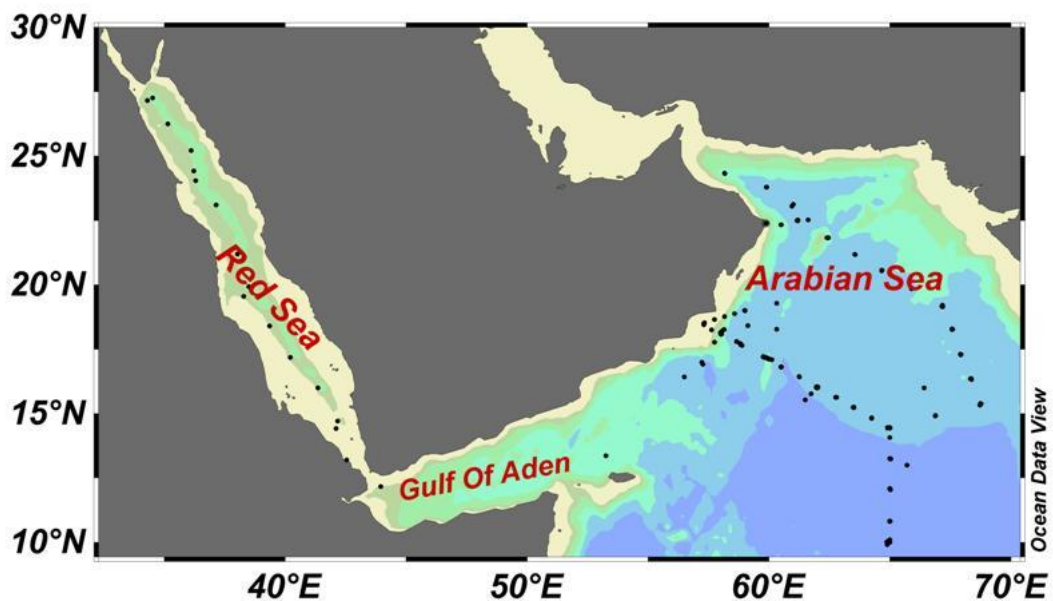


FIGURE 5.1: A map of the Arabian Sea and the Red Sea with stations indicated.

5.1.1 JGOFS Cruises data 1995

The US Joint Global Ocean Flux Studies (JGOFS) Arabian Sea Expedition (1994–1995) (Figure 5.2) was a comprehensive study of the biogeochemistry and plankton dynamics of the Arabian Sea (Campbell et al., 1998; Flagg and Kim, 1998; Garrison et al., 1998; Marra and Barber, 2005)

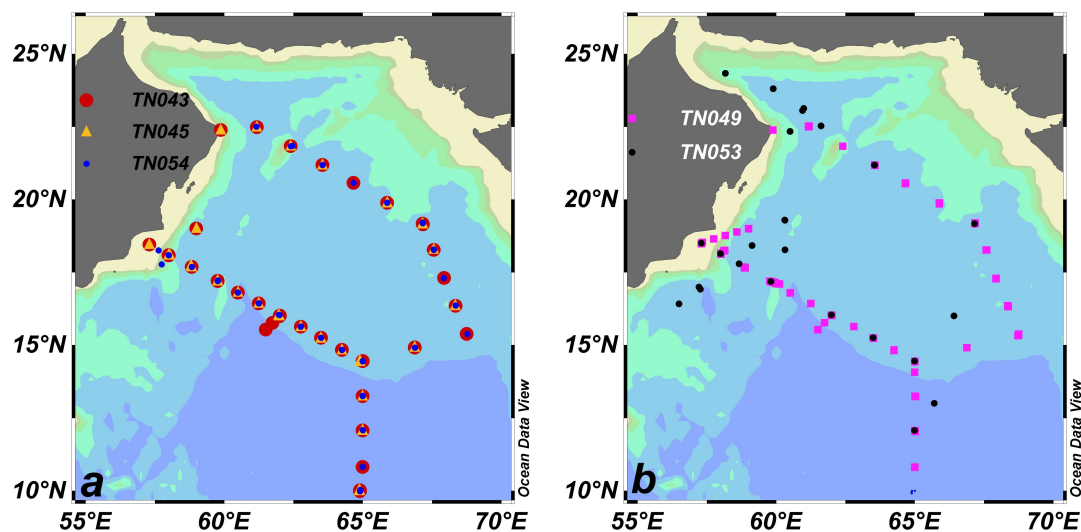


FIGURE 5.2: Stations collected at the JGOFS Arabian Sea cruises during (a) winter and (b) summer.

The measurements of TA, DIC, and related variables reported here were collected during the five cruises (Table 5.1): TN043, TN045, TN049, TN053, and TN054 (Figure 5.2). These periods correspond to late NE monsoon (L NE), Spring Intermonsoon (SI), mid SW monsoon (M SW), Fall Intermonsoon (FI) and early NE monsoon (E NE) (see Table 5.1) (Buesseler et al., 1998; Johnson et al., 2002; Sambrotto, 2001). In general, each cruise track followed the standard US JGOFS Arabian Sea plan that provided access to coastal water along the Omani coast, deeper waters under the seasonal Findlater Jet and tropical oligotrophic regions. Discrete water samples were collected from 10 liter Niskin bottles on a rosette. All samples were shielded from bright light with opaque sampling vessels and carriers (Johnson et al., 2002). The precision of the data were ± 3.2 and ± 2.7 mol kg⁻¹ for TA and DIC, respectively (Millero et al., 1998).

5.1.2 GEOSECS data 1977

Geochemical Ocean Section Study (GEOSECS) was a global survey of the three-dimensional distribution of chemical, isotopic, and radiochemical tracers in the ocean. The samples were collected during 19th to 27th of December 1977 by R/V ATLANTIS II from five stations in the Red Sea and Gulf of Aden (Figure 5.3) (Østlund and Stuiver, 1988). According to Bradshaw et al. (1981) the error of the DIC data was +12 mol kg⁻¹, while the TA data did not have any offset. The variables which were determined are listed in Table 5.1.

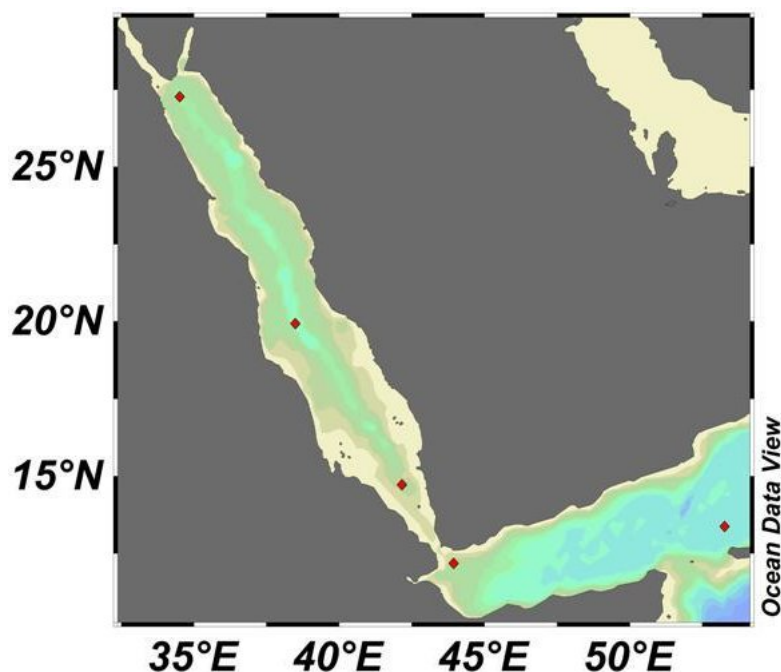


FIGURE 5.3: GEOSECS 1977 stations in the Red Sea and Gulf of Aden.

5.1.3 MEROU cruise data 1982

The Mer Rouge (MEROU) data were obtained during two cruises with R/V MARION DUFRESNE; first from 16th of June to 4th of July 1982 (A) and then from 25th of September to 9th of October 1982 (B). The cruises focused on the regime of summer monsoon in the Red Sea and the nearby Gulf of Aden to make an estimate of carbon balance in the strait of Bab el Mandeb, and also to study the variation of the system overall on a longitudinal section in the Red Sea (Figure 5.4).

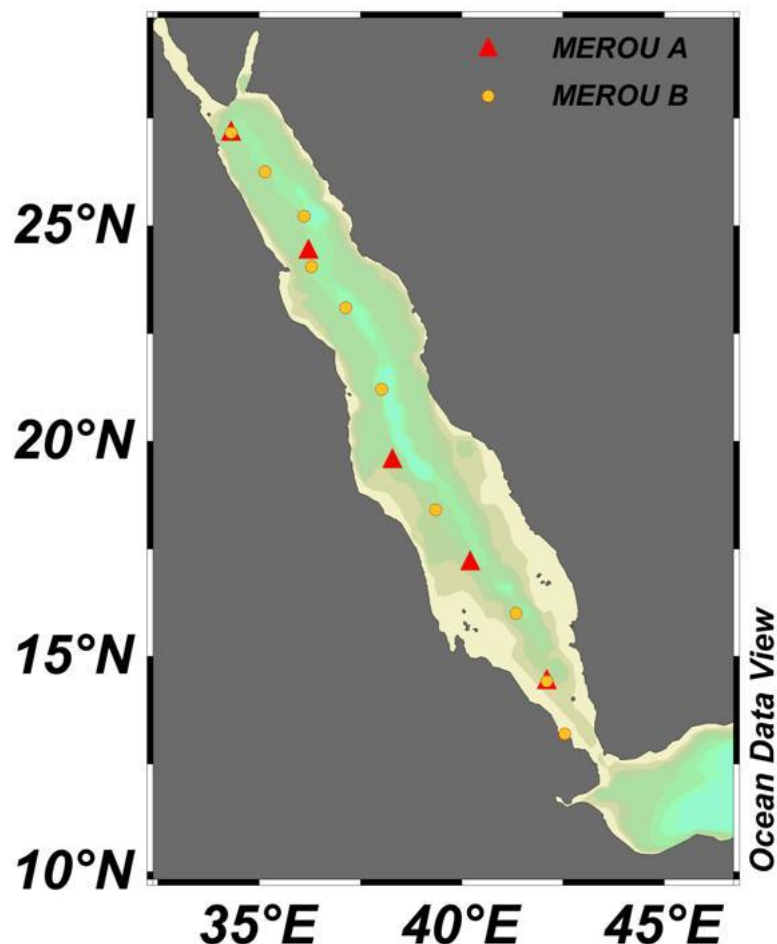


FIGURE 5.4: MEROU 1982 cruises in the Red Sea.

The sampled data are listed in Table 5.1. TA and DIC were determined using a potentiometric method derived from the procedure described by [Dyrssen and Sillén \(1967\)](#) and improved by [Bradshaw et al. \(1981\)](#) with an accuracy of respectively 0.1 and 0.3%. The nutrients (nitrite NO_2 , nitrate NO_3 , silicate SiO_3 , and phosphate PO_4) were titrated on an automatic apparatus of the Technicon type according to a method recommended by [Tréguer and Le Corre \(1975\)](#), with an accuracy of respectively 1, 0.3, 0.3, and 0.5%. Oxygen was titrated by the Winkler method ([Carpenter, 1965](#)), with an accuracy of 1%, and temperature had an accuracy of 0.005°C ([Papaud and Poisson, 1986](#)).

TABLE 5.1: Summary of the Arabian and Red Seas datasets

Data Set	Cruise	Dates mm/dd/yy	Monsoon /Season Period	T (°C)	S	TA (μeq /kg)	DIC (μmol /kg)	pH	O ₂ (μmol /kg)	AOU (μmol /kg)	PO ₄ (μmol /kg)	NO ₂ (μmol /kg)	NO ₃ (μmol /kg)	SIO ₃ (μeq /kg)
JGOFS	TN043	01/08– 02/11/95	L NE	+	+	+	+	–	+	–	+	+	+	+
JGOFS	TN045	03/14– 04/08/95	SI	+	+	+	+	+	+	–	–	–	–	–
JGOFS	TN049	07/18– 08/13/95	M SW	+	+	+	+	–	+	–	+	+	+	+
JGOFS	TN053	10/29– 11/25/95	FI	+	+	+	+	–	+	–	–	–	+	–
JGOFS	TN054	11/30– 12/28/95	E NE	+	+	+	+	+	+	–	–	–	–	–
GEOSECS	ATLANTIS II	12/19– 12/27/77	winter	+	+	+	+	–	+	+	+	+	+	+
MEROU	MARION DUFRESNE	A: 06/16– 07/04/82 B: 09/25– 10/09/82	summer	+	+	+	+	–	–	+	+	+	+	+

(+) means that the parameter has been measured during the cruise, while (–) refer to parameters not measured.

5.2 Methods

In addition to the measured data we used the CO2SYS program by [Lewis and Wallace \(1998\)](#) with the constants of [Mehrbach et al. \(1973\)](#) to calculate some additional variables of the carbonate system. These were pH, the carbonate ion concentration (CO_3^{2-}), fCO_2 , the Revelle Factor (R) and the degree of saturation for aragonite (Ω_{Ar}) and calcite (Ω_{Ca}). Also, Apparent Oxygen Utilization (AOU) was determined as the difference between the measured oxygen and the saturation concentration.

For the quantification of TA changes due to different processes, the water occupying the depth layer 160–200 m in the Arabian Sea was chosen as the reference water or source water i.e. water with TA values that has not been affected neither by surface processes (e.g. evaporation, dilution by freshwater and production of organic matter and CaCO_3) nor deep water processes (e.g. destruction of organic matter and CaCO_3). In other words, it was assumed that this is the water that wells up and joins the surface circulation in both the Arabian Sea and the Red Sea. Henceforth, properties of the source water will be identified with superscript r . The total change in TA due to different processes mentioned in Chapter 4 is given by:

$$\Delta\text{TA} = \Delta\text{TA}^{org} + \Delta\text{TA}^S + \Delta\text{TA}^{CaCO_3} \quad (5.1)$$

where ΔTA^{org} , ΔTA^S , and ΔTA^{CaCO_3} are the contribution arising from organic matter production/remineralisation, salinity variations, and matter production/dissolution of calcium carbonate, respectively. ΔTA^{org} was computed from nitrate change (ΔNO_3) by assuming that for each mole nitrate consumed/remineralized TA increase/decreases by one mole ([Brewer and Goldman, 1976](#)). For each sample, ΔNO_3 was determined as the difference between nitrate concentration in the source water (ΔNO_3^r) and the measured concentration (ΔNO_3).

$$\Delta\text{TA}^{org} = \text{NO}_3^r - \text{NO}_3 \quad (5.2)$$

ΔTA^S was estimated from salinity variations. This was achieved by identifying the salinity-TA relationship for each region using the surface alkalinity data that has been corrected for organic matter ($\Delta\text{TA}^{cor} = \text{TA} + \Delta\text{TA}^{org}$). That is, by regressing

ΔTA^{cor} data with salinity. The slope of the resulting linear relationship quantifies the change in TA per each unit salinity change, while the intercept indicates the significance of other sources and sinks of TA (Friis et al., 2003). Thus, we have

$$\Delta\text{TA}^{cor} = aS + b \quad (5.3)$$

$$\Delta\text{TA}^{cor\ r} = aS^r + b \quad (5.4)$$

$$\Delta\text{TA}^S = \text{TA}^{cor\ r} - \text{TA}^{cor} = a(S^r - S) \quad (5.5)$$

ΔTA^{CaCO_3} has been estimated by first adjusting TA^{cor} from all depths to constant salinity i.e. that of the source water, S^r . This is done by solving equation 5.3 for a and substituting into equating 5.4 (Friis et al., 2003, 2007; Omar et al., 2005) so that:

$$n\text{TA} = \text{TA}^{cor\ r} = (\text{TA}^{cor} - b) \frac{S^r}{S} + b \quad (5.6)$$

where $n\text{TA}$ is the organic matter and salinity normalized TA. According to equation 5.6 if only organic matter and salinity variations influence TA i.e. if $\Delta\text{TA}^{CaCO_3} = 0$ then $n\text{TA}$ for each sample will be equal to the nitrate corrected TA of the source water, $\text{TA}^{cor\ r}$. If not the difference is assumed to be due to ΔTA^{CaCO_3} so that:

$$\Delta\text{TA}^{CaCO_3} = n\text{TA} - \text{TA}^{cor\ r} \quad (5.7)$$

Negative values of indicate formation of calcium carbonate whereas positive values indicate dissolution (Goyet et al., 1999).

All the processes mentioned above also influence DIC and total change is given by:

$$\Delta\text{DIC} = \Delta\text{DIC}^{org} + \Delta\text{DIC}^S + \Delta\text{DIC}^{CaCO_3} \quad (5.8)$$

where ΔDIC^{org} , ΔDIC^S , and $\Delta\text{DIC}^{CaCO_3}$ are the contribution arising from organic matter production/remineralisation, salinity variations, and matter production/dissolution of calcium carbonate, respectively. ΔDIC^{org} was computed from nitrate change (ΔNO_3) by assuming that for each 16 moles of nitrate consumed/remineralized DIC decreases/increases by 106 moles (Redfield et al., 1963).

$$\Delta\text{DIC}^{org} = \frac{106}{16} (\text{NO}_3^r - \text{NO}_3) \quad (5.9)$$

$\Delta\text{DIC}^{\text{CaCO}_3}$ has been computed from $\Delta\text{TA}^{\text{CaCO}_3}$ by realizing that from each mole TA change due to CaCO_3 precipitation/dissolution half a mole of DIC would follow (see equations 3.6 and 3.4). Then we have

$$\Delta\text{DIC}^{\text{CaCO}_3} = 0.5\Delta\text{TA}^{\text{CaCO}_3} \quad (5.10)$$

ΔDIC^S has been estimated by assuming that DIC data for which $\Delta\text{DIC}^{\text{CaCO}_3}$ and $\Delta\text{TA}^{\text{org}}$ have been accounted i.e. $\Delta\text{DIC}^{\text{cor}}$ varies only due to salinity variations in the manner depicted by equation 5.3. Then

$$n\text{DIC} = \text{DIC}^{\text{cor } r} = (\text{DIC}^{\text{cor}} - b) \frac{S^r}{S} + b \quad (5.11)$$

where

$$\begin{aligned} \text{DIC}^{\text{cor}} &= \text{DIC} - \Delta\text{DIC}^{\text{org}} - \Delta\text{DIC}^{\text{CaCO}_3} \\ &= \text{DIC} + \frac{106}{16} (\text{NO}_3^r - \text{NO}_3) - 0.5 (n\text{TA} - \text{TA}^{\text{cor } r}) \end{aligned} \quad (5.12)$$

According to equation 5.11 if organic matter, salinity variations, and calcium carbonate are the only processes that influence TA, $n\text{DIC}$ for each sample will be equal to $n\text{DIC}$ of the source water. Any deviations from this suggest additional processes driving DIC changes. One obvious candidate is air-sea gas exchange. Therefore, the biggest deviations are expected for the surface samples.

Chapter 6

Result and discussion

The contributions of different processes to TA variations in the Arabian and Red Seas are presented in the following three sections. Also, the effect of these processes on DIC was quantified as described in Chapter 5 where it was implied that $nDIC$ should be constant with depth. In the last section deviation from this expected constancy in $nDIC$ is quantified and discussed.

6.1 Salinity control on TA

The distribution of total alkalinity, TA, in the upper 50 m in the two basins is shown together with the salinity in Figure 6.1. The Arabian Sea shows larger variation in TA and salinity values during summer compared to winter, while in the Red Sea the winter is the season with largest TA and salinity variations. The Arabian Sea has a minimum in TA and salinity in the upwelling region at the Omani coast, while the maxima of TA occur in the Gulf of Oman during summer (Figures 6.1a and 6.1b). In the Red Sea, the lowest TA and salinity occur in the south, due to influx of fresher water from Gulf of Aden, and the values increases northwards. In general, higher TA and salinity values are found in the Red Sea compared to the Arabian Sea.

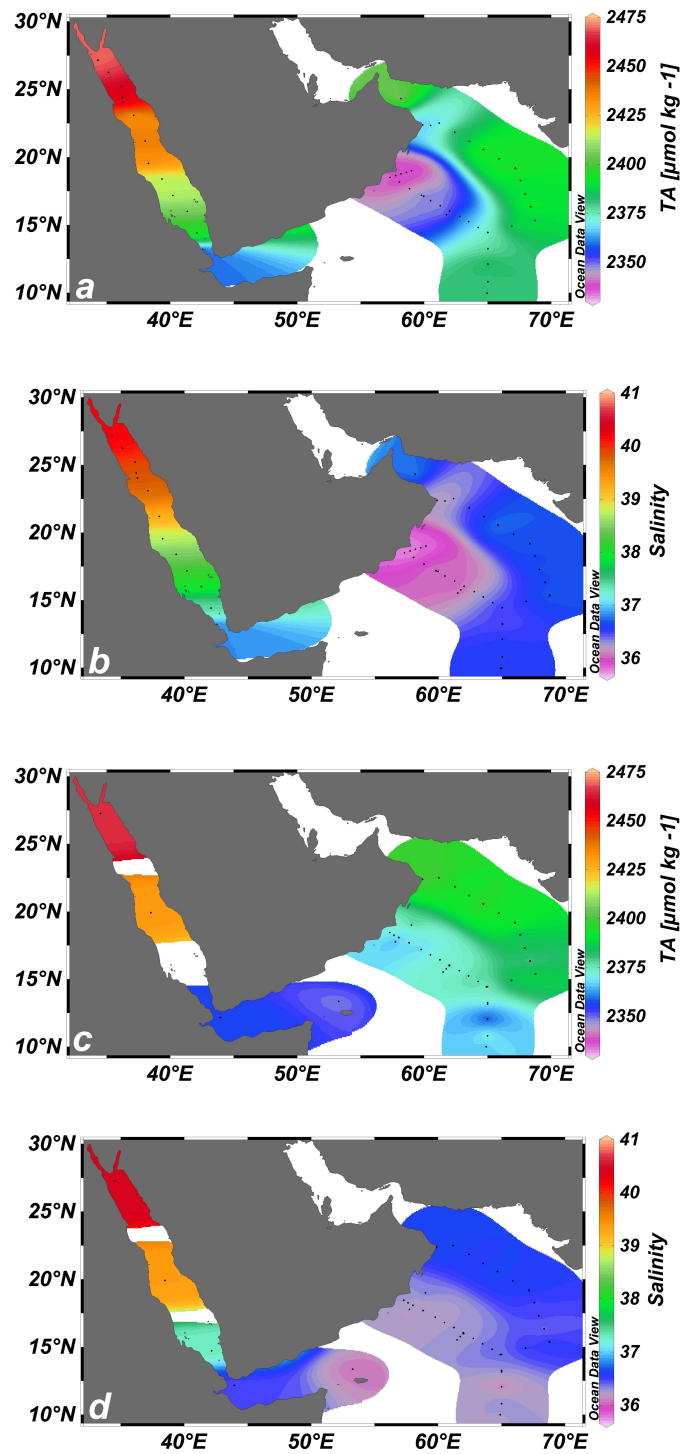


FIGURE 6.1: Surface TA and SSS during summer (a) and (b) and winter (c) and (d) in the Red and the Arabian Sea.

Alkalinity is a major component of seawater and the distribution of surface TA is strongly correlated with SSS. This is seen overall in the surface the Arabian and Red Seas (Figure 6.2a). The variation in SSS is connected to several processes such as annual evaporation exceeding precipitation, fresh water dilution by upwelling in the Arabian Sea, and influx of relatively fresh water from Gulf of Aden into the Red Sea. Two different regimes are also evident from Figure 6.2a. As the salinity increases from that of the source water (38) due to evaporation, the alkalinity increases in both seas. However, a lower increase is seen in the Red Sea, which indicates additional processes removing alkalinity in this area. This will be further elaborated in Section 6.3.

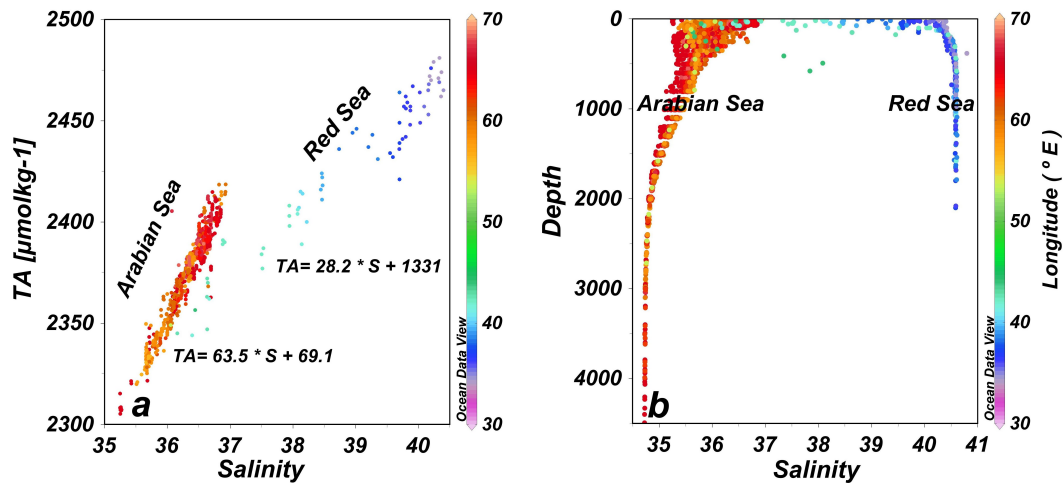


FIGURE 6.2: (a) Relationship between TA and salinity in the upper 50 m and (b) vertical distribution of salinity.

Figure 6.2b shows salinity profiles from the two seas in this study. In the upper 200 m the salinity varies by about 1.7 in the Arabian Sea and 4 in the Red Sea. Using the slopes determined in Figure 6.2a of 63.5 and 28.2 for the Arabian Sea and Red Sea, respectively, we calculate that the surface water salinity variations are responsible for TA changes of about $70 \mu\text{mol kg}^{-1}$ and $121 \mu\text{mol kg}^{-1}$ in the Arabian Sea and Red Sea, respectively. Below 200 m salinity variations are responsible for TA changes of about $45 \mu\text{mol kg}^{-1}$ in the Arabian Sea and $6 \mu\text{mol kg}^{-1}$ in the Red Sea.

The alkalinity data shown in Figure 6.2a includes effects of organic matter production and calcification, which result in slightly biased slopes in the figure. To

perform these corrections values for the source water are needed. These are presented in Table 6.1, which also shows corrected slopes for the alkalinity-salinity relationships. The impacts of additional processes influencing TA are presented in the following sections.

TABLE 6.1: Mean values and standard deviations for the salinity (S), total alkalinity (TA), nitrate (NO_3), and total carbon (DIC) for the source water. Also shown are slopes (a) and intercepts (b) for TA^{cor} versus S relationships in the Arabian Sea and the Red Sea.

Area	Depth ranges	S	NO_3	TA	DIC	a	b
Source water	160–200	35.8 ± 0.20	23.8 ± 8	2339 ± 57	2239	–	–
Arabian Sea	0–50	–	–	–	–	48	608.5
Red Sea	0–50	–	–	–	–	26.8	1362.4

6.2 Impact of organic matter on TA

Production and remineralisation of organic matter produces an inverse correlation between TA and NO_3 as can be seen from Figures 6.3a and 6.3b. The figure shows data between 50 and 600 m, since this is the depth range where most of the remineralisation of organic matter occurs. In the surface, for instance, the salinity control on TA is the dominant process and can conceal the expected inverse relationship between TA and NO_3 . Below 600 m, on the other hand, dissolution of CaCO_3 starts to become dominant and conceal the expected inverse relationship between TA and NO_3 . Therefore, 50–600 m is the depth layer where one can see the organic matter effect on TA clearest.

The impact of organic matter on TA i.e. ΔTA^{org} vary between around 0 and $24 \mu\text{mol kg}^{-1}$ in the upper 200 m (Figure 6.4). For depths below 200 m, ΔTA^{org} vary between -10 and $0 \mu\text{mol kg}^{-1}$ in the Arabaian Sea, and between 0 and $10 \mu\text{mol kg}^{-1}$ in the Red Sea. Hence, in the surface the impact of organic matter on TA is much less than that of salinity, but below 200 m the two effects are comparable in magnitude.

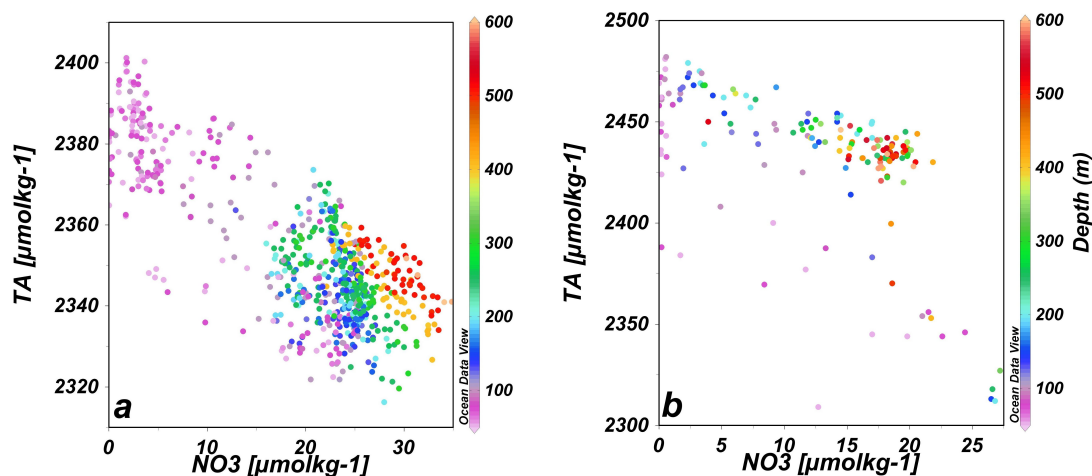


FIGURE 6.3: Relationship between TA and NO_3 in the depth range 50–600 m in the (a) Arabian Sea and (b) Red Sea.

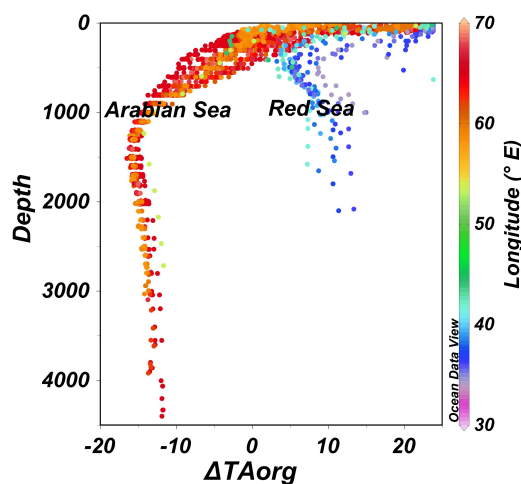


FIGURE 6.4: Change in alkalinity due to production/remineralisation of organic matter, ΔTA^{org} in the Arabian Sea and Red Sea.

DIC is also affected by photosynthesis and remineralisation. The change of DIC versus nitrate is much higher compared to TA. The stoichiometry of the seawater can be an indicator of DIC changes due to nutrient consumption during photosynthesis in the surface water or release during remineralisation processes in the water column. Figure 6.5 shows the DIC and nitrate concentration, respectively, in the upper 50 m in the Arabian and Red Seas. In contrast to TA, the DIC and NO_3 are high in the summer at the upwelling region along the Omani coast (Figures 6.5a and 6.5b) and low during winter over the two basins (Figures 6.5c and 6.5d).

The high DIC values in the upwelling region is due to the the enrichment of the CO_2 . Elsewhere in the Arabian Sea the surface DIC is distributed uniformly. The coincidence of low surface DIC and high O_2 reflects the high primary production (not shown here).

In Red Sea, DIC is maximum in the north basin and decrease southwards during both seasons.

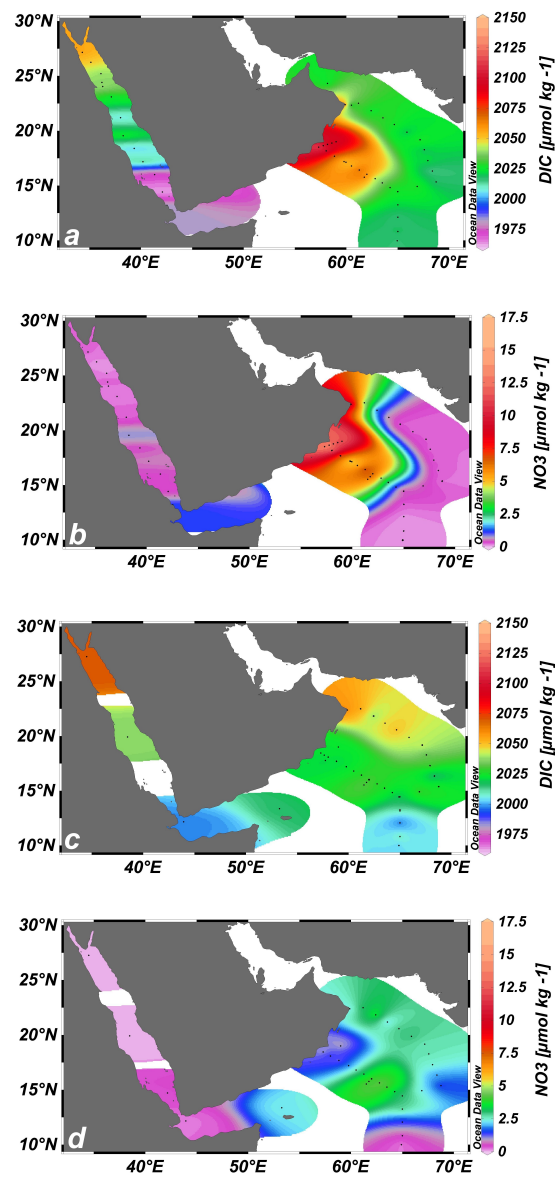


FIGURE 6.5: Surface DIC and nitrate during (a and b) summer and (c and d) winter in the Red and Arabian Seas.

The surface values for DIC and nutrients are low due to biological production, and in the deep, values are enriched due to remineralization (Figure 6.6). This gives rise to the strong co-variation between DIC and nutrients that is depicted in Figure 6.6. A remarkable feature for the DIC versus NO_3 for the Arabian Sea (Figure 6.6a) is the deviation from the line for samples with low O_2 . In these low oxygen samples, nitrogen is produced and lost to the atmosphere during remineralization by a processes known as denitrification. During this process, DIC increases without a concurrent increase in NO_3 . The result is the feature observed in Figure 6.6.

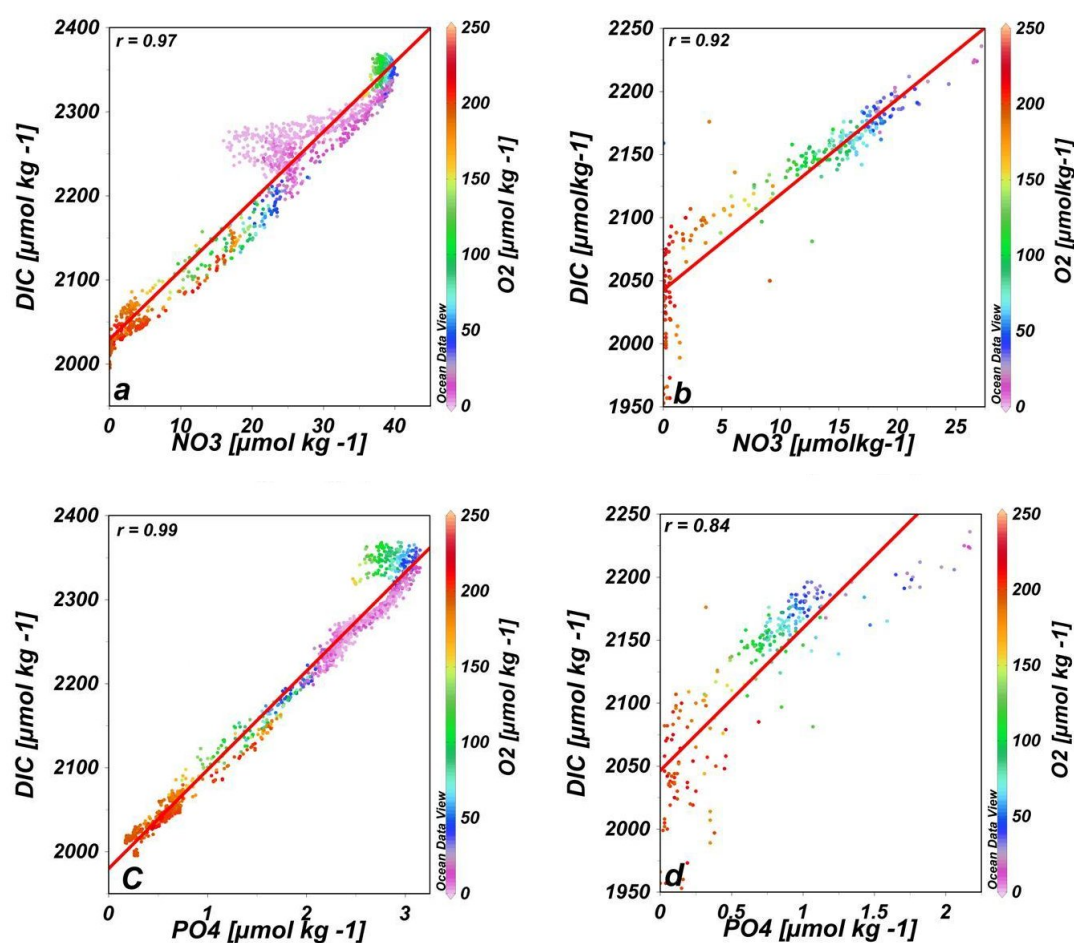


FIGURE 6.6: C: N and C: P ratios in the Arabian Sea (a and c) and the Red Sea (b and d). The colour indicates Oxygen concentration.

6.3 CaCO₃ cycle and saturation depths

The formation and dissolution of CaCO₃ is one of the important processes controlling the concentration of DIC and TA in both surface and deep ocean. In surface waters plankton convert dissolved bicarbonate ions to CaCO₃ and dissolved carbon dioxide. In deep water some of the CaCO₃ (either calcitic foraminifera or coccolithic debris) dissolves and the remainder is buried in the sediments. The lack of aragonitic sediments in deeper waters is simply due to the fact that aragonite is much more soluble than calcite.

Surface waters of the two basins are found to be supersaturated with respect to CaCO₃ (Figure 6.7 and Figure 6.8) with higher values for calcite than those for aragonite. There are seasonal and regional variations. The degree of saturation varied between 2.5–5 for Ω_{Ar} and between 3.5–7.9 for Ω_{Ca} . Our data demonstrated a higher degree of saturation in the Red Sea surface water compared to the Arabian Sea surface. In addition, the summer turns out to be the season with the highest saturation degree. An exception of this is the upwelling region along the Omani coast which has the lowest saturation degree as well as lowest CO₃²⁻. In summer, the Red Sea surface is heavily supersaturated because of the warm oligarchic waters which enhance the coral reef growth, while Arabian Sea surface Ω values decrease due to upwelling (Figures 6.7a and 6.8a). The minimum saturation level in the southern Red Sea during winter (Figures 6.7b and 6.8b) is connected to the influx of relatively fresh water, which promotes dissolution of CO₃²⁻ and hampers CaCO₃ formation (Chierici and Fransson, 2009).

The degree of saturation decreases with increasing depth in the two basins (Figures 6.9a and 6.9b). The Arabian Sea is found to become undersaturated with respect to aragonite and calcite at around 400 and 3000 m, respectively, which permit carbonate mineral to dissolve below these depths. Conversely, the level of undersaturation is never reached in the Red Sea. Therefore, sedimentation of CaCO₃ out of the water column is possible in the Red Sea.

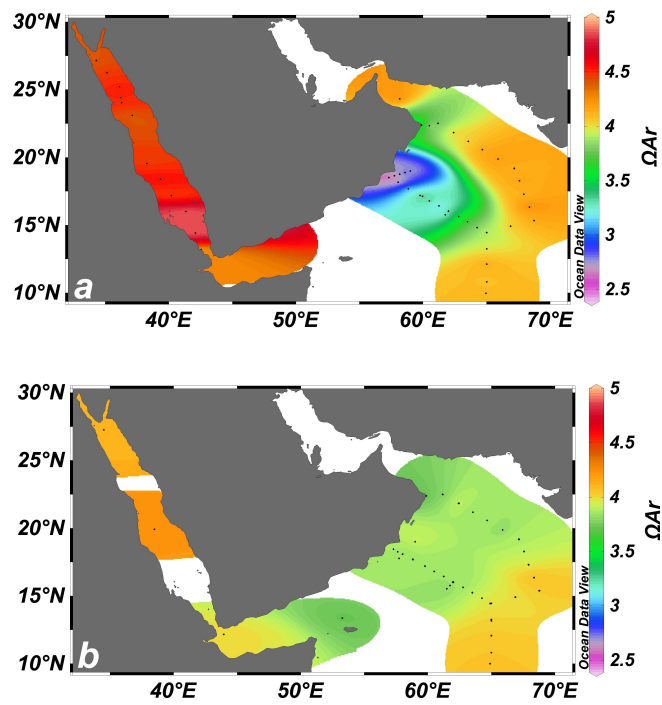


FIGURE 6.7: Degree of saturation with respect to aragonite during (a) summer and (b) winter in the Red Sea and the Arabian Sea.

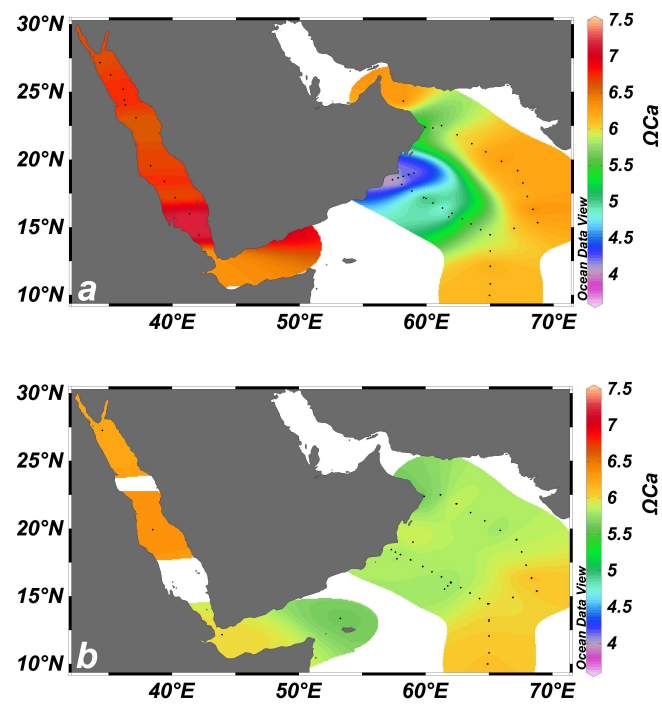


FIGURE 6.8: Degree of saturation with respect to calcite during (a) summer and (b) winter in the Red Sea and the Arabian Sea.

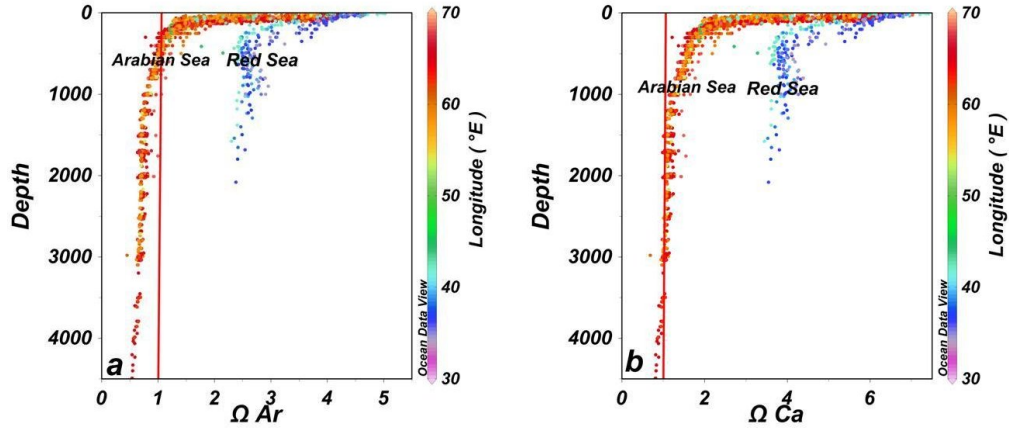


FIGURE 6.9: Depth profiles of the degree of saturation (Ω) of (a) aragonite and (b) calcite in the Arabian Sea and Red Sea. The Red lines indicate that the degree of saturation equals One.

Depth variations of nTA are mainly due to formation of calcium carbonate in the upper ocean and dissolution in subsurface and deep parts of the water column. In the Red Sea nTA decreases almost monotonically until 1000 m and then stabilizes around $2300 \mu\text{mol kg}^{-1}$. In the Arabian Sea nTA increases with depth (Figure 6.10a). Profiles of ΔTA^{CaCO_3} (Figure 6.10b) show negative values at upper layers during calcium carbonate formation and positive in deeper waters during its dissolution, this is the circumstances in the Arabian Sea whilst the Red Sea has negative values of TA^{CaCO_3} all way to the bottom. This relates to high calcification rates and high degrees of saturation in this sea. Therefore, sedimentation of calcium carbonate minerals probably takes place, which lowers the alkalinity in the Red Sea deep water (Metzl et al., 1989).

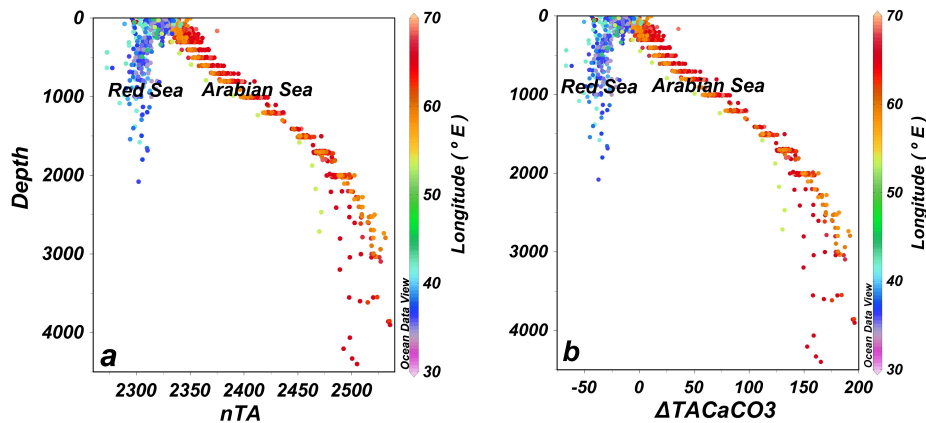


FIGURE 6.10: (a) nTA and (b) ΔTA^{CaCO_3} as function of depth in the Red Sea and the Arabian Sea. The colour indicates longitude.

The depth profiles of $n\text{DIC}$ are shown in Figure 6.11a. Below 1000 m $n\text{DIC}$ is nearly constant at in both seas. This is according to the expectations and it confirms that all processes that contribute to the depth variations of DIC were accounted for (see Chapter 5). Conversely, from 1000 m to about 160 m, $n\text{DIC}$ increases to values higher than its deep water values. This is a manifestation of the process of denitrification (Section 6.2) which has not been accounted for when computing $n\text{DIC}$. Furthermore, from 160 m and to the surface $n\text{DIC}$ decreases to values less than its deep water values. Again, this is due to air-sea exchange which decreases DIC in the upper layer of the water column. This statement is supported by the strong correlation between the carbon loss and temperature (Figure 6.11b), the carbon loss equal $n\text{DIC} - 2239$, where 2239 is the mean value of DIC in source water. The reason for this correlation is that as water upwells to the surface and start circulate in the Arabian Sea while its temperature increases. At the same time $n\text{DIC}$ decreases as the water loose more and more carbon.

The fact that $n\text{DIC}$ deviates from the expected constancy due to the above mentioned two processes lend confidence to the computations of $n\text{TA}$ in this thesis. This is because TA is independent on air-sea gas exchange, and the theoretical contribution of denitrification on TA variability is maximum $15 \mu\text{mol kg}^{-1}$ (i.e 7 times less than that in DIC). Therefore, one can be confident that in this thesis all processes significantly influencing TA have been considered.

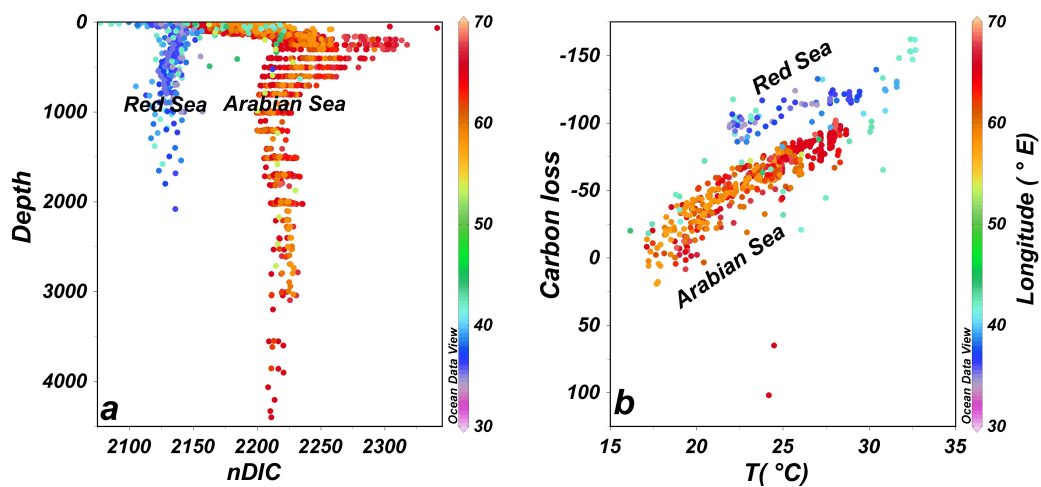


FIGURE 6.11: (a) $n\text{DIC}$ as a function of depth and (b) relation between carbon loss and temperature in upper 160 m in the Red Sea and Arabian Sea. The colour indicates longitude.

Summary of results

In this thesis, we have summarized the factors driving the TA changes in the Arabian Sea and Red Sea; these factors include physical factors such as salinity, mixing, and circulation pattern, and biological factors such as photosynthesis, remineralization, calcium carbonate formation, precipitation, and dissolution.

The surface distribution of TA was dictated by that of salinity and hence two different linear relationships between TA and salinity were identified for the two seas. The TA-salinity relationship for the Red Sea had a lower slope compared to that of the Arabian Sea, and this was attributed to loss of TA by CaCO_3 production and probably also due to sedimentation. Another remarkable feature of the surface distribution of TA was the minimum values along the Omani coast in the Arabian Sea which was connected to upwelling of deep water with lower salinity (and hence TA).

The degree of saturation for aragonite (Ω_{Ar}) and calcite (Ω_{Ca}) in the Arabian Sea surface were 3.4 ± 0.8 and 5.1 ± 1.2 , respectively, with minimum values near the Omani coast in summer due to upwelling of CO_2 enriched and less saline deep water. In the Red Sea surface, the mean summer values for Ω_{Ar} and Ω_{Ca} were 4.2 ± 0.7 and 6.3 ± 0.9 , respectively, with higher values in the south and north. This was attributed to the high biological productivity in the south and the high temperature in the center of the Red Sea. During winter, Ω_{Ar} and Ω_{Ca} were somewhat lower (4.12 ± 0.02 and 6.2 ± 0.15 , respectively) with highest values in the central due to the high temperatures in this region.

The Arabian Sea was found to be undersaturated with respect to aragonite and calcite at around 400 and 3000 m, respectively. Conversely, the level of undersaturation was never reached in the Red Sea. Therefore, sedimentation of CaCO_3 out of the water column is possible in the Red Sea.

Alkalinity variations were composed of contributions arising from salinity variations (ΔTA^s), organic matter production/remineralisation (ΔTA^{org}), and production/dissolution of calcium carbonate (ΔTA^{CaCO_3}). In the upper 200 m, alkalinity changes due to salinity were $70 \mu\text{mol kg}^{-1}$ and $121 \mu\text{mol kg}^{-1}$ for the Arabian Sea and the Red Sea, respectively. Below this depth for the Arabian Sea, ΔTA^s was $45 \mu\text{mol kg}^{-1}$, while the Red Sea had a ΔTA^s value of $6 \mu\text{mol kg}^{-1}$. Changes in TA due to organic matter production and remineralization, ΔTA^{org} , is at the largest ($24 \mu\text{mol kg}^{-1}$) in the Arabian and Red Sea surface waters. Deeper than 200 m, the Arabian Sea had ΔTA^{org} values between -10 and $0 \mu\text{mol kg}^{-1}$, while in the Red Sea, it varied between 0 and $10 \mu\text{mol kg}^{-1}$. Contribution from calcium carbonate formation/dissolution, ΔTA^{CaCO_3} , were about $0 \mu\text{mol kg}^{-1}$ in the surface in both seas. In the Arabian Sea the ΔTA^{CaCO_3} increased approximately linearly with depth until about 3000 m, where it reached and stabilized at around $150 \mu\text{mol kg}^{-1}$. The increase was attributed to calcium carbonate dissolution, which was connected to the undersaturation with respect to aragonite and calcite at about 400 and 3000 m, respectively. In the Red Sea, on the other hand, ΔTA^{CaCO_3} decreased with depth and stabilized to a value of $-40 \mu\text{mol kg}^{-1}$ at about 500 m. This is due to formation of CO_3 and sedimentation in this basin, which removed TA from the water column.

Bibliography

- Abdel Aleem, A., J. Morgan, and P. Verlaan (2009), Arabian Sea. In Encyclopedia Britannica. Retrieved April, 2009, from Encyclopedia Britannica Online: <http://www.britannica.com/EBchecked/topic/31653/Arabian-Sea>, last visited April 2009.
- Aiki, H., K. Takahashi, and T. Yamagata (2006), The Red Sea outflow regulated by the Indian monsoon, *Continental Shelf Research*, *26*(12–13), 1448–1468.
- Al Saafani, M., and S. Shenoi (2004), Seasonal cycle of hydrography in the Bab el Mandab region, southern Red Sea, *Journal of Earth System Science*, *113*(3), 269–280.
- Ali, E. (2008), The Inorganic Carbon Cycle in the Red Sea, Master Thesis in Chemical Oceanography, Master’s thesis, University of Bergen.
- Anschutz, P., and G. Blanc (1996), Heat and salt fluxes in the Atlantis II Deep (Red Sea), *Earth and Planetary Science Letters*, *142*(1-2), 147–159.
- Archer, D. (1996), An atlas of the distribution of calcium carbonate in sediments of the deep sea, *Global Biogeochemical Cycles*, *10*(1), 159–174.
- Background, T. (2007), Electrochemical acceleration of chemical weathering as an energetically feasible approach to mitigating anthropogenic climate change, *Environmental Science and Technology*, *41*(24), 8464–8470.
- Bates, N., A. Michaels, and A. Knap (1996), Alkalinity changes in the Sargasso Sea: geochemical evidence of calcification?, *Marine Chemistry*, *51*(4), 347–358.

- Berner, R., M. Scott, and C. Thomlinson (1970), Carbonate alkalinity in the pore waters of anoxic marine sediments, *Limnology and Oceanography*, 15(4), 544–549.
- Bonfil, R., and M. Abdallah (2004), *Field identification guide to the sharks and rays of the Red Sea and Gulf of Aden*, Food and Agriculture Organization.
- Bradshaw, A., P. Brewer, D. Shafer, and R. Williams (1981), Measurements of total carbon dioxide and alkalinity by potentiometric titration in the GEOSECS program, *Earth and Planetary Science Letters*, 55(1), 99–115.
- Brand, T., and C. Griffiths (2009), Seasonality in the hydrography and biogeochemistry across the Pakistan margin of the NE Arabian Sea, *Deep-Sea Research Part II*, 56(6–7), 283–295.
- Brewer, P., and J. Goldman (1976), Alkalinity changes generated by phytoplankton growth, *Limnology and Oceanography*, 21(1), 108–117.
- Buesseler, K., L. Ball, J. Andrews, C. Benitez-Nelson, R. Belostock, F. Chai, and Y. Chao (1998), Upper ocean export of particulate organic carbon in the Arabian Sea derived from thorium-234, *Deep-Sea Research Part II*, 45(10–11), 2461–2487.
- Campbell, L., M. Landry, J. Constantinou, H. Nolla, S. Brown, H. Liu, and D. Caron (1998), Response of microbial community structure to environmental forcing in the Arabian Sea, *Deep-Sea Research Part II*, 45(10–11), 2301–2325.
- Carpenter, J. (1965), The Chesapeake Bay Institute technique for the Winkler dissolved oxygen method, *Limnology and Oceanography*, 10(1), 141–143.
- Chierici, M., and A. Fransson (2009), Calcium carbonate saturation in the surface water of the Arctic Ocean: undersaturation in freshwater influenced shelves, *Biogeosciences*, 6(11), 2421–2431.
- Chowdary, J., C. Gnanaseelan, B. Thompson, and P. Salvekar (2005), Water mass properties and transports in the Arabian Sea from Argo observations, *Journal of Atmospheric and Ocean Science*, 10(3), 235–260.

- De Pol-Holz, R., R. Robinson, D. Hebbeln, D. M. Sigman, and O. Ulloa (2009), Controls on sedimentary nitrogen isotopes along the Chile margin, *Deep-Sea Research Part II*, 56(16), 1100–1112.
- DeSousa, S., M. DileepKumar, S. Sardesai, V. Sarma, and P. Shirodkar (1996), Seasonal variability in oxygen and nutrients in the central and eastern Arabian Sea, *Current Science*, 71(11), 847–851.
- Dickey, T., J. Marra, D. Sigurdson, R. Weller, C. Kinkade, S. Zedler, J. Wiggert, and C. Langdon (1998), Seasonal variability of bio-optical and physical properties in the Arabian Sea: October 1994–October 1995, *Deep-Sea Research Part II*, 45(10–11), 2001–2025.
- Dickson, A., and C. Goyet (1994), Handbook of methods for the analysis of the various parameters of the carbon dioxide system in sea water, *ORNL/CDIAC-74*.
- Douabul, A., and A. Haddad (1999), *The Red Sea and Yemen's Red Sea Environments*, 1-16 pp., Douabul, A., T.S. Roupael and R. Marchant (eds.). Hassell and Assoc., AMSAT and UNOPS.
- Dyrssen, D., and L. Sillén (1967), Alkalinity and total carbonate in sea water. A plea for pX-independent data, *Tellus*, 19(1), 113–121.
- Edwards, F. (1987), *Climate and oceanography*. In: *The Red Sea*, 45–70 pp., Edwards, A.J. and S.M. Head (eds). Pergamon press, Oxford.
- Egleston, E., C. Sabine, and F. Morel (2010), Revelle revisited: Buffer factors that quantify the response of ocean chemistry to changes in DIC and alkalinity, *Global Biogeochemical Cycles*, GB1002, 24(1), doi:10.1029/2008GB003407.
- Emerson, S., and D. Archer (1990), Calcium carbonate preservation in the ocean, *Philosophical Transactions of the Royal Society of London. Series A, Mathematical and Physical Sciences*, 331, 29–40.
- Feely, R., C. Sabine, K. Lee, W. Berelson, J. Kleypas, V. Fabry, and F. Millero (2004), Impact of anthropogenic CO₂ on the CaCO₃ system in the oceans, *Science*, 305, 362–366.

- Flagg, C., and H. Kim (1998), Upper ocean currents in the northern Arabian Sea from shipboard ADCP measurements collected during the 1994–1996 US JGOFS and ONR programs, *Deep-Sea Research Part II*, 45(10–11), 1917–1959.
- Friis, K., A. Körtzinger, and D. Wallace (2003), The salinity normalization of marine inorganic carbon chemistry data, *Geophysical Research Letters*, 30(2), doi:10.1029/2002GL015898.
- Friis, K., R. Najjar, M. Follows, S. Dutkiewicz, A. Körtzinger, and K. Johnson (2007), Dissolution of calcium carbonate: observations and model results in the subpolar North Atlantic, *Biogeosciences*, 4, 205–213.
- Galy, A., and C. France-Lanord (1999), Weathering processes in the Ganges-Brahmaputra basin and the riverine alkalinity budget, *Chemical Geology*, 159(1–4), 31–60.
- Gangstø, R., M. Gehlen, B. Schneider, L. Bopp, O. Aumont, and F. Joos (2008), Modeling the marine aragonite cycle: changes under rising carbon dioxide and its role in shallow water CaCO₃ dissolution, *Biogeosciences*, 5, 1057–1072.
- Garrison, D., M. Gowing, and M. Hughes (1998), Nano-and microplankton in the northern Arabian Sea during the Southwest Monsoon, August–September 1995 A USJGOFS study, *Deep-Sea Research Part II*, 45(10–11), 2269–2299.
- Gordon, L., and L. Jones (1973), The effect of temperature on carbon dioxide partial pressures in seawater, *Marine Chemistry*, 1(4), 317–322.
- Goyet, C., C. Coatanoan, G. Eiseid, T. Amaoka, K. Okuda, R. Healy, and S. Tsunogai (1999), Spatial variation of total CO₂ and total alkalinity in the northern Indian Ocean: A novel approach for the quantification of anthropogenic CO₂ in seawater, *Journal of Marine Research*, 57(1), 135–163.
- Hasan, M. (2009), Stock assessment of holothuroid populations in the Red Sea waters of Saudi Arabia, *SPC Beche-de-mer Information Bulletin*, 29, 31–37.
- Heinze, C., E. Maier-Reimer, and K. Winn (1991), Glacial pCO₂ reduction by the world ocean: Experiments with the Hamburg carbon cycle model, *Paleoceanography*, 6(4), 395–430.

- Honjo, S., and R. Weller (1997), Monsoon winds and carbon cycles in the Arabian Sea, *Oceanus*, 40, 24–28.
- Iglesias-Rodriguez, M., P. Halloran, R. M. Rickaby, I. Hall, E. Colmenero-Hidalgo, J. Gittins, D. Green, T. Tyrrell, S. Gibbs, and P. Von Dassow (2008), Phytoplankton calcification in a high-CO₂ world, *Science*, 320, 336–340.
- Ilyina, T., R. Zeebe, E. Maier-Reimer, and C. Heinze (2009), Early detection of ocean acidification effects on marine calcification, *Global Biogeochemical Cycles*, 23. GB1008, doi:10.1029/2008GB003278.
- Jean-Baptiste, P., E. Fourre, N. Metzl, J. Terner, and A. Poisson (2004), Red Sea deep water circulation and ventilation rate deduced from the ³He and ¹⁴C tracer fields, *Journal of Marine Systems*, 48(1–4), 37–50.
- Johnson, Z., R. Bidigare, R. Goericke, J. Marra, C. Trees, and R. Barber (2002), Photosynthetic physiology and physicochemical forcing in the arabian sea, 1995, *Deep-Sea Research Part I*, 49(3), 415–436.
- Jones, I., and C. Lu (2003), *Engineering Carbon Sequestration in the Ocean*, presented at the Second Annual Conference on Carbon Sequestration, Washington.
- Kempe, S., and J. Kazmierczak (1994), The role of alkalinity in the evolution of ocean chemistry, organization of living systems, and biocalcification processes, *Bulletin de l'Institut océanographique*, pp. 61–117.
- Kinsey, D. (1978), Alkalinity changes and coral reef calcification, *Limnology and Oceanography*, 23(5), 989–991.
- Kleypas, J., and C. Langdon (2006), Coral reefs and changing seawater carbonate chemistry, *Coral reefs and climate change: science and management. Coast Estuar Stud*, 61, 73–110.
- Kotb, M., M. Abdulaziz, Z. Al-Agwan, K. Alshaikh, H. Al-Yami, A. Banajah, L. Devantier, M. Eisinger, M. Eltayeb, M. Hassan, et al. (2004), 4. Status of coral reefs in the Red Sea and Gulf of Aden in 2004, *Status of coral reefs of the world*, 1, 137–154.

- Kumar, M. (2006), *Biogeochemistry of the North Indian Ocean*, 25 pp., Indian National Science Academy: IGBP-WCRP-SCOPE Report Series: 1, appears in Collections: Interdisciplinary Oceanography.
- Langdon, C., T. Takahashi, C. Sweeney, D. Chipman, J. Goddard, F. Marubini, H. Aceves, H. Barnett, and M. Atkinson (2000), Effect of calcium carbonate saturation state on the calcification rate of an experimental coral reef, *Global Biogeochemical Cycles*, 14(2), 639–654.
- Lee, C., B. Jones, K. Brink, and A. Fischer (2000), The upper-ocean response to monsoonal forcing in the Arabian Sea: seasonal and spatial variability, *Deep Sea Research Part II: Topical Studies in Oceanography*, 47(7–8), 1177–1226.
- Lee, K., L. Tong, F. Millero, C. Sabine, A. Dickson, C. Goyet, G. Park, R. Wanninkhof, R. Feely, and R. Key (2006), Global relationships of total alkalinity with salinity and temperature in surface waters of the world's oceans, *Geophysical Research Letters*, 33, L19,605.
- Lewis, E., and D. Wallace (1998), Program developed for CO₂ system calculations, *ORNL/CDIAC-105. Carbon Dioxide Information Analysis Center, Oak Ridge National Laboratory, US Department of Energy, Oak Ridge, Tennessee.*
- Luis, A., and H. Kawamura (2004), Air-sea interaction, coastal circulation and primary production in the eastern Arabian Sea: a review, *Journal of Oceanography*, 60(2), 205–218.
- Marra, J., and R. Barber (2005), Primary productivity in the Arabian Sea: A synthesis of JGOFS data, *Progress in Oceanography*, 65(2–4), 159–175.
- Mehrbach, C., C. Culberson, J. Hawley, and R. Pytkowicz (1973), Measurement of the apparent dissociation constants of carbonic acid in seawater at atmospheric pressure, *Limnology and Oceanography*, 18(6), 897–907.
- Metzl, N., B. Moore Iii, A. Papaud, and A. Poisson (1989), Transport and carbon exchanges in Red Sea inverse methodology, *Global Biogeochemical Cycles*, 3(1), 1–26.

- Millero, F., E. Degler, D. O'Sullivan, C. Goyet, and G. Eiseid (1998), The carbon dioxide system in the Arabian Sea, *Deep-Sea Research Part II*, 45(10–11), 2225–2252.
- Morcos, S. (1970), Physical and chemical oceanography of the Red Sea, *Oceanography and Marine Biology Annual Review* 8, pp. 73–202.
- Morcos, S., and G. Soliman (1974), Circulation and deep water formation in the northern Red Sea in winter, *L'océanographie Physique de la Mer Rouge, (IAPSO Symposium), Publications du CNEXO, Paris*, 2, 91–103.
- Morrison, J., L. Codispoti, S. Smith, K. Wishner, C. Flagg, W. Gardner, S. Gaurin, S. W. Naqvi, V. Manghnani, and L. Prosperie (1999), The oxygen minimum zone in the Arabian Sea during 1995, *Deep-Sea Research Part II*, 46(8–9), 1903–1931.
- Murray, S., and W. Johns (1997), Direct observations of seasonal exchange through the Bab el Mandab Strait, *Geophysical Research Letters*, 24(21), 2557–2560.
- Naqvi, S., H. Bange, S. Gibb, C. Goyet, A. Hatton, and R. Upstill-Goddard (2005), Biogeochemical ocean-atmosphere transfers in the Arabian Sea, *Progress in Oceanography*, 65(2–4), 116–144.
- Nozaki, Y., and T. Oba (1995), Dissolution of calcareous tests in the ocean and atmospheric carbon dioxide, *Biogeochemical Processes and Ocean Flux in the Western Pacific*, pp. 83–92.
- Omar, A., T. Johannessen, R. Bellerby, A. Olsen, L. Anderson, and C. Kivimae (2005), Sea-Ice and Brine Formation in Storfjorden: Implications for the Arctic Wintertime Air-Sea CO₂ Flux, *Geophysical Monograph-American Geophysical Union*, 158, 177–187.
- Østlund, H., and M. Stuiver (1988), GEOSECS Atlantic, Pacific, Indian, and Mediterranean Radiocarbon DATA: <http://cdiac.ornl.gov/ftp/ndp027/ndp027.doc>, doi:10.3334/CDIAC/otg.ndp027.
- Papaud, A., and A. Poisson (1986), Distribution of dissolved CO₂ in the Red Sea and correlations with other geochemical tracers, *Journal of Marine Research*, 44(2), 385–402.

- Patzert, W. (1974), Wind-induced reversal in Red Sea circulation, in *Deep Sea Research and Oceanographic Abstracts*, vol. 21, pp. 109–121, Elsevier.
- Perrings, C. (2009), Biodiversity Conservation in Sea Areas Beyond National Jurisdiction: The Economic Problem, *Conserving and valuing ecosystem services and biodiversity: economic, institutional and social challenges*, pp. 59–65.
- PERSGA (2004), The Regional Organization for the Conservation of the Environment of the Red Sea and Gulf of Aden, website: <http://www.persga.org> (Accessed March 2009).
- Post, W., T. Peng, W. Emanuel, A. King, V. Dale, and D. DeAngelis (1990), The global carbon cycle, *American Scientist*, 78(4), 310–326.
- Prasad, T., M. Ikeda, and S. Kumar (2001), Seasonal spreading of the Persian Gulf Water mass in the Arabian Sea, *Journal of Geophysical Research*, 108(C8), 17,059–17,071.
- Rasheed, M., M. Badran, C. Richter, and M. Huettel (2002), Effect of reef framework and bottom sediment on nutrient enrichment in a coral reef of the Gulf of Aqaba, Red Sea, *Marine Ecology Progress Series*, 239, 277–285.
- Redfield, A., B. Ketchum, and F. Richards (1963), *The influence of organisms on the composition of sea-water*. Hill, M.N. (ed.), 26–77 pp., Interscience, New York.
- Riebesell, U., I. Zondervan, B. Rost, P. Tortell, R. Zeebe, and F. Morel (2000), Reduced calcification of marine plankton in response to increased atmospheric CO₂, *Nature*, 407(6802), 364–367.
- Rohling, E., and W. Zachariasse (1996), Red Sea outflow during the last glacial maximum, *Quaternary International*, 31, 77–83.
- Sabine, C., R. Key, R. Feely, and D. Greeley (2002), Inorganic carbon in the Indian Ocean: Distribution and dissolution processes, *Global Biogeochemical Cycles*, 16(4), 1067, doi: 10.1029/2002GB001,869.
- Sambrotto, R. (2001), Nitrogen production in the northern Arabian Sea during the Spring Intermonsoon and Southwest Monsoon seasons, *Deep-Sea Research Part II*, 48(6–7), 1173–1198.

- Sarmiento, J., and N. Gruber (2006), *Ocean biogeochemical dynamics*, 526 pp., Princeton University Press.
- Schlesinger, W. (1997), *Biogeochemistry: An analysis of global change*, 2nd ed., 588 pp., Academic Press, San Diego.
- Schott, F., J. McCreary, et al. (2001), The monsoon circulation of the Indian Ocean, *Progress in Oceanography*, *51*(1), 1–123.
- Schulz, K., J. e Ramos, R. Zeebe, and U. Riebesell (2009), CO₂ perturbation experiments: similarities and differences between dissolved inorganic carbon and total alkalinity manipulations, *Biogeosciences*, *6*, 2145–2153.
- Shetye, S., A. Gouveia, and S. S. Shenoi (1994), Circulation and water masses of the Arabian Sea, *Journal of Earth System Science*, *103*(2), 107–123.
- Shimmield, G., N. Price, and T. Pedersen (1990), The influence of hydrography, bathymetry and productivity on sediment type and composition of the Oman Margin and in the Northwest Arabian Sea, *Geological Society London Special Publications*, *49*, 759–769, doi:10.1144/GSL.SP.1992.049.01.46.
- Siddall, M., D. Smeed, S. Matthiesen, and E. Rohling (2002), Modelling the seasonal cycle of the exchange flow in Bab el Mandab (Red Sea), *Deep Sea Research Part I: Oceanographic Research Papers*, *49*(9), 1551–1569.
- Sigman, D., and E. Boyle (2000), Glacial/interglacial variations in atmospheric carbon dioxide, *Nature*, *407*(6806), 859–869.
- Smith, S., and M. Madhupratap (2005), Mesozooplankton of the Arabian Sea: patterns influenced by seasons, upwelling, and oxygen concentrations, *Progress in Oceanography*, *65*(2–4), 214–239.
- Sofianos, S., and W. Johns (2003), An Oceanic General Circulation Model (OGCM) investigation of the Red Sea circulation: 2. Three-dimensional circulation in the Red Sea, *Journal of Geophysical Research-Oceans*, *108*(C3), doi:10.1029/2001JC001185.
- Tomczak, M., and J. Godfrey (1994), *Regional Oceanography: An Introduction*, Pergamon Press, New York.

- Tomczak, M., and J. Godfrey (2001), *Regional oceanography: an introduction*, Oxford.
- Tréguer, P., and P. Le Corre (1975), Manuel d'analyse des sels nutritifs dans l'eau de mer, *Laboratoire d'Océanographie Chimique, Université de Bretagne Occidentale, Brest*, 110.
- Vecchi, G., S. Xie, and A. Fischer (2004), Ocean-atmosphere covariability in the western Arabian Sea, *Journal of Climate*, 17(6), 1213–1224.
- Weiss, R. (1974), Carbon dioxide in water and seawater: the solubility of a non-ideal gas, *Marine Chemistry*, 2(3), 203–215.
- Werner, F., and K. Lange (1975), A Bathymetric Survey of the Sill Area between the Red Sea and the Gulf of Aden, *Geologische Jahrbuch*, 13, 125–130.
- Woelk, S., and D. Quadfasel (1996), Renewal of deep water in the Red Sea during 1982–1987, *Journal of Geophysical Research-Oceans*, 101(C8), 18,155–18,165.
- Wolf-Gladrow, D., J. Bijma, and R. Zeebe (1999), Model simulation of the carbonate chemistry in the microenvironment of symbiont bearing foraminifera, *Marine Chemistry*, 64(3), 181–198.
- Wolf-Gladrow, D., R. Zeebe, C. Klaas, A. Körtzinger, and A. Dickson (2007), Total alkalinity: the explicit conservative expression and its application to biogeochemical processes, *Marine Chemistry*, 106(1), 287–300.
- Yamanaka, Y., and E. Tajika (1996), The role of the vertical fluxes of particulate organic matter and calcite in the oceanic carbon cycle: Studies using an ocean biogeochemical general circulation model, *Global Biogeochemical Cycles*, 10(2), 361–382.
- Zeebe, R., and D. A. Wolf-Gladrow (2001), *CO₂ in Seawater: Equilibrium, kinetics, isotopes*, Elsevier Science Ltd.
- Zhifei, L., X. Jian, T. Jun, and W. Pinxian (2003), Calcium carbonate pump during Quaternary glacial cycles in the South China Sea, *Chinese Science Bulletin*, 48(17), 1862–1869.

Zondervan, I., R. Zeebe, B. Rost, and U. Riebesell (2001), Decreasing marine biogenic calcification: A negative feedback on rising atmospheric pCO₂, *Global Biogeochemical Cycles*, 15(2), 507–516.